

Adsorption and Transformation of Acetaldehyde on the TiO₂ Surface

Von der Naturwissenschaftlichen Fakultät der
Gottfried Wilhelm Leibniz Universität Hannover

zur Erlangung des Grades

Doktorin der Naturwissenschaften

(Dr. rer. nat.)

genehmigte Dissertation

von

Stephanie Melchers, M. Sc.

2019

Referent: apl. Prof. Dr. rer. nat. habil. Detlef W. Bahnemann

Korreferent: Prof. Dr. rer. nat. Jürgen Caro

Tag der Promotion: 16.04.2019

Für meine Familie

Danksagung

Zunächst möchte ich Herrn Prof. Dr. Bahnemann dafür danken, dass er es mir ermöglicht hat in seinem Arbeitskreis zu promovieren. Außerdem danke ich ihm für die Betreuung meiner Doktorarbeit und dass er mir die Freiheit gegeben hat eigene Ideen zu entwickeln und umzusetzen.

Herrn Prof. Dr. Caro danke ich für die Bereitschaft der Übernahme des Korreferats.

Herrn Prof. Dr. Scheper danke ich für die Möglichkeit an seinem Institut promoviert haben zu können und für die Übernahme des Promotionsvorsitzes.

Ganz besonders bedanken möchte ich mich außerdem bei Frau Dr. Jenny Schneider für die wertvollen und produktiven Diskussionen und die dabei entstandenen neuen Ideen, welche meine Arbeit wesentlich geprägt haben.

Ich danke dem gesamten TCI für das tolle Arbeitsklima, eine schöne Zusammenarbeit und für eine unvergessliche Zeit.

Besonders danken möchte ich meinen Freunden und Kollegen Ana, Arsou, Lena, Maryam, Camilla, Christoph, Manuel, Fabian und Carsten.

Zuallerletzt möchte ich meinem Freund Björn und meiner Familie dafür danken, dass sie mich stets motiviert und unterstützt haben.

Kurzzusammenfassung

Während des letzten Jahrzehnts wurde intensiv im Bereich der Photokatalyse geforscht, denn Photokatalysatoren wie beispielsweise Titandioxid (TiO_2) können mit Hilfe von UV Licht die Zersetzung organischer Schadstoffe in Abwässern und in der Luft katalysieren. Trotz intensiver Forschung gibt es jedoch nur vergleichsweise wenige Untersuchungen zu den grundlegenden Reaktionsmechanismen des photokatalytischen Abbaus in der Literatur, obwohl das Verständnis dieser Prozesse essentiell ist, um neue Photokatalysatoren mit höherer photokatalytischer Aktivität zu entwickeln.

Im Rahmen dieser Arbeit wurde der Einfluss von O_2 und H_2O auf die Adsorption und den Abbauprozess von Acetaldehyd auf der TiO_2 Oberfläche im Dunkeln und unter UV-Strahlung untersucht. Hierbei wurden die Prozesse auf der TiO_2 Oberfläche mit Hilfe der *in situ* ATR-FTIR Spektroskopie untersucht, während die Gasphase mittels GC/PID und MS analysiert wurde. Die erhaltenen Ergebnisse wurden miteinander korreliert, um ein besseres Verständnis von den Adsorptions- und den Abbauprozessen von Acetaldehyd auf der TiO_2 Oberfläche zu erhalten.

Es wird in dieser Arbeit gezeigt, dass im Dunkeln eine durch die TiO_2 Oberfläche katalysierte Aldolkondensation von zwei adsorbierten Acetaldehydmolekülen zu Crotonaldehyd stattfindet. Die Reaktion wird dabei stark von der Luftfeuchtigkeit beeinflusst, denn bei Zunahme der Luftfeuchtigkeit sinken die Adsorption von Acetaldehyd und damit ebenfalls die Bildung von Crotonaldehyd. Im Gegensatz dazu hat die Anwesenheit von O_2 keinen Einfluss auf die Oberflächenprozesse im Dunkeln. Es zeigt sich jedoch, dass O_2 einen großen Effekt auf die Zersetzung von Acetaldehyd unter UV-Strahlung hat, denn in Abwesenheit von O_2 wird Acetaldehyd nur unvollständig abgebaut. Neben dem Einfluss von O_2 wird in dieser Arbeit mit Hilfe von Ti^{18}O_2 gezeigt, dass Sauerstoffatome aus dem TiO_2 Gitter am photokatalytischen Abbau von Acetaldehyd beteiligt sind.

Stichwörter: Titandioxid, Acetaldehyd, Adsorption, Abbaumechanismus, Gittersauerstoff.

Abstract

During the last decade intensive research work has been carried out in the field of photocatalysis because upon UV illumination photocatalysts such as titanium dioxide (TiO_2) are able to catalyze the degradation of organic compounds in waste water as well as in air. However, the reaction mechanisms and the limitations of the photocatalytic processes have been studied in the literature less frequently, although the understanding of the fundamental processes is essential in order to design a photocatalyst with an improved photocatalytic activity.

In this work the effect of O_2 and H_2O on the adsorption and the photocatalytic degradation of gaseous acetaldehyde over TiO_2 has been investigated in the dark and upon UV illumination. The surface processes have been elucidated by means of *in situ* ATR-FTIR spectroscopy, while the gas phase was analysed by GC/PID and MS. The results obtained from the surface and from the gas phase were correlated with each other in order to gain a deeper insight into the adsorption and the degradation mechanism of acetaldehyde.

In this study it is shown, that in the dark the TiO_2 surface is able to catalyze an aldol condensation of two adsorbed acetaldehyde molecules forming crotonaldehyde. These surface processes are strongly affected by the humidity, because an increasing water vapor content induces a decrease in the adsorption of acetaldehyde molecules resulting in a reduction of the crotonaldehyde formation. In contrast, molecular O_2 does not exhibit an influence on the surface processes in the dark. However, upon UV illumination the degradation of acetaldehyde is strongly affected by the O_2 concentration, because acetaldehyde is incompletely degraded when O_2 is not present. Besides the important role of O_2 , isotopic studies using Ti^{18}O_2 show that lattice oxygen atoms from the TiO_2 surface are involved in the photocatalytic degradation process of acetaldehyde in the absence of O_2 .

Keywords: titanium dioxide, acetaldehyde, adsorption, degradation mechanism, lattice oxygen.

Table of contents

1	Introduction and objectives.....	1
2	Theoretical background	5
2.1	Titanium dioxide	5
2.2	Surface structure of TiO ₂	7
2.3	Acetaldehyde in the dark.....	8
2.4	Acetaldehyde upon UV illumination	10
2.5	Role of lattice oxygen atoms in photocatalytic reactions.....	12
3	Materials and experimental methods	15
3.1	Materials.....	15
3.2	Experimental methods.....	15
3.2.1	Specific surface area measurements	15
3.2.2	Raman spectroscopy	15
3.2.3	X-ray diffraction	15
3.2.4	Field-emission scanning electron microscopy	16
3.2.5	Attenuated total reflection Fourier-transform infrared spectroscopy	16
3.2.6	Gas chromatography / photoionization detector.....	19
3.2.7	Mass spectrometry	20
3.2.8	TiO ₂ film preparation.....	21
4	Results.....	23
4.1	Characterization of the TiO ₂ powders.....	23
4.1.1	Raman spectroscopy	23
4.1.2	X-ray diffraction	24
4.1.3	Scanning electron microscopy	24
4.2	Acetaldehyde adsorption and crotonaldehyde formation on the TiO ₂ surface in the dark	25
4.3	Adsorption of acetaldehyde and formation of crotonaldehyde on the TiO ₂ surface in the presence of water vapor in the dark	29

4.4	Adsorption of acetaldehyde and formation of crotonaldehyde on the anatase surface in the presence and absence of O ₂ in the dark	32
4.5	Photocatalytic degradation of acetaldehyde in the presence and absence of molecular O ₂	33
4.6	Photodesorption of crotonaldehyde from the TiO ₂ surface	36
4.7	Evolution of gaseous products during the photocatalytic degradation of acetaldehyde over TiO ₂ in the absence of molecular O ₂	37
5	Discussion	45
5.1	Acetaldehyde adsorption and crotonaldehyde formation under dry conditions in the dark.....	45
5.2	Effect of water vapor on the adsorption of acetaldehyde and the formation of crotonaldehyde	47
5.3	Effect of O ₂ on the adsorption of acetaldehyde and the formation of crotonaldehyde	49
5.4	Photodesorption of crotonaldehyde from the TiO ₂ surface	51
5.5	Acetaldehyde degradation in O ₂ and N ₂ atmosphere.....	53
6	Summary and conclusions.....	63
7	References	67
8	Publications	72
9	Curriculum vitae.....	73

Abbreviations

ATR	Attenuated Total Reflection
BET	Specific Surface Area according to Brunauer Emmet Teller
BG	Bandgap
CB	Conduction Band
DTGS	Deuterated Triglycine Sulfate Detector
E	Energy
FE-SEM	Field-Emission Scanning Electron Microscopy
FTIR	Fourier Transform Infrared
GC	Gas Chromatography
IRE	Internal Reflection Element
MS	Mass spectrometry
NHE	Normal Hydrogen Electrode
NMR	Nuclear Magnetic Resonance
PID	Photoionization Detector
PMMA	Polymethylmethacrylate
POIE	Photoinduced Oxygen Isotopic Exchange
ppb	Parts per Billion
ppm	Parts per Million
QMS	Quadrupole Mass Spectrometer
Ref	Reference
RH	Relative Humidity
RT	Room Temperature
STM	Scanning Tunneling Microscopy
TOF	Time of Flight
TPD	Temperature Programmed Desorption
UV	Ultraviolet
VB	Valence Band
VIS	Visible
XRD	X-ray Diffraction

1 Introduction and objectives

Nowadays, the demand for clean and fresh air and water is a public health issue, because the rising energy consumption has led to an increase of toxic agents in water as well as in air. In this regard, one major indoor air pollutant is acetaldehyde released by building materials such as polyurethane foams, and consumer products such as cigarettes, adhesives, coatings and inks.¹ In Europe and in the USA occupational exposure levels are set for acetaldehyde, because it is a potential human carcinogen.^{2,3} In order to decrease the concentration of this air pollutant, photocatalysis might be a sustainable and environmentally friendly solution because upon UV(A) illumination titanium dioxide (TiO₂) is able to catalyze the decomposition of organic compounds yielding CO₂, H₂O and traces of mineral acids as reaction products.⁴ Despite intensive research work in the field of photocatalysis during the past years the photocatalytic activity is still not sufficient for a widespread application. For the design of a photocatalyst with an improved photocatalytic activity, the reaction mechanisms and the involved limitations need to be understood.

Hence, in this work, the adsorption and the photocatalytic degradation of acetaldehyde on the TiO₂ surface are investigated in the dark and upon UV illumination. The processes occurring on the TiO₂ surface are monitored by means of *in situ* ATR-FTIR (Attenuated Total Reflection - Fourier Transform Infrared) spectroscopy, while GC/PID (gas chromatography/photoionization detector) and MS (mass spectrometry) allow the detection of gas phase products.

In situ ATR-FTIR spectroscopy is an established technique that provides a deeper understanding of the interfacial processes occurring at the semiconductor/liquid and semiconductor/gas interface. This technique allows to monitor the adsorption of molecules on a solid surface as well as the detection of intermediates and products formed during the photocatalytic process.^{5,6}

Employing FTIR spectroscopy, it has been shown that under dry conditions in the dark, a surface catalyzed aldol condensation of two acetaldehyde molecules forming crotonaldehyde takes place on the TiO₂ surface.^{7,8} Batault *et al.*⁹ showed that under dry conditions in the dark acetaldehyde is mostly irreversibly adsorbed on the TiO₂ surface, while at 50 % relative humidity (RH) acetaldehyde adsorption only occurs as a reversible

1 Introduction and objectives

physical adsorption. The effect of water vapor on the formation of crotonaldehyde has not been discussed in literature.

Only a few studies have been published concerning the degradation mechanism of acetaldehyde on the TiO₂ surface upon UV illumination. Muggli *et al.*¹⁰ and Ohko *et al.*¹¹ investigated the degradation of acetaldehyde over TiO₂ in the presence of molecular O₂ and upon weak UV illumination. According to their proposed reaction mechanism (see Figure 1.1) acetaldehyde is firstly oxidized into acetic acid, which is followed by a decarboxylation yielding CO₂ and formaldehyde. Formaldehyde is then oxidized into formic acid and eventually to CO₂.

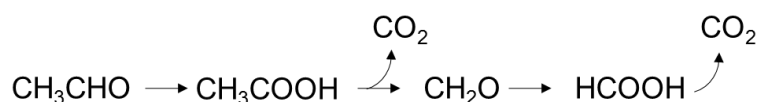


Figure 1.1: Proposed reaction mechanism for the degradation of acetaldehyde over TiO₂ in the presence of O₂ and upon weak UV illumination. Reprinted from Ref.¹²

The degradation mechanism of gaseous acetaldehyde over TiO₂ in the absence of molecularly O₂ has not been reported in literature. In photocatalysis O₂ plays an important role, because it acts as an electron scavenger preventing charge carrier recombination and it is also involved in the oxidation reactions of organic compounds.¹³

For a better understanding of the photocatalytic conversion of acetaldehyde on the TiO₂ surface, in this work the effect of water vapor and molecular O₂ on the adsorption of acetaldehyde and the formation of crotonaldehyde on the TiO₂ is investigated in the dark. Furthermore, acetaldehyde is photocatalytically degraded over TiO₂ in the presence and absence of O₂ in order to elucidate how molecular O₂ affects the degradation mechanism of acetaldehyde.

Besides the important role of O₂ and water in photocatalytic oxidation reactions, the involvement of lattice oxygen atoms from the TiO₂ surface should also be taken into account in understanding photocatalysis.¹⁴ In the literature the role of lattice oxygen atoms from the TiO₂ surface during photocatalytic oxidation reactions has not been clarified yet. Montoya *et al.*¹⁵ evidenced an incorporation of lattice oxygen atoms into CO₂ during the photocatalytic degradation of benzene over isotopically labelled Ti¹⁸O₂ under anaerobic conditions. In contrast, other studies reported no participation of lattice oxygen atoms in photocatalytic reactions.^{16,17}

In order to clarify whether lattice oxygen atoms from the TiO_2 surface are involved in photocatalytic gas phase reactions, isotopic studies using Ti^{18}O_2 are performed. Herein, acetaldehyde is degraded over Ti^{16}O_2 and the isotopologues Ti^{18}O_2 upon UV illumination in the absence of O_2 and the evolved gaseous products C^{16}O_2 and $\text{C}^{18}\text{O}^{16}\text{O}$ are detected by MS. The incorporation of lattice oxygen atoms into CO_2 is elucidated by a comparison between the $\text{C}^{18}\text{O}^{16}\text{O}/\text{C}^{16}\text{O}_2$ ratio of Ti^{18}O_2 and Ti^{16}O_2 .

1 Introduction and objectives

2 Theoretical background

This chapter will first present the basic principles and mechanisms of photocatalysis on the TiO_2 surface. The surface structure and the adsorption properties of the TiO_2 surface are described in detail, because photocatalytic reactions take place on the surface. Furthermore, the adsorption and the photocatalytic degradation of the air pollutant acetaldehyde on the TiO_2 surface are described in the dark and upon UV illumination. At the end, the involvement of lattice oxygen atoms from the TiO_2 surface in photocatalytic reactions is described.

2.1 Titanium dioxide

TiO_2 exists in three different crystalline modifications: anatase, rutile, and brookite. Brookite and anatase are metastable and can be converted into the thermodynamically most stable phase rutile by increasing the pressure and/or the temperature. As illustrated in Figure 2.1 the three polymorphs consist of TiO_6 octahedra. Anatase and rutile crystallize in a tetragonal unit cell, while brookite exhibits an orthorhombic cell structure. The different unit cell structures result in varying physicochemical properties.

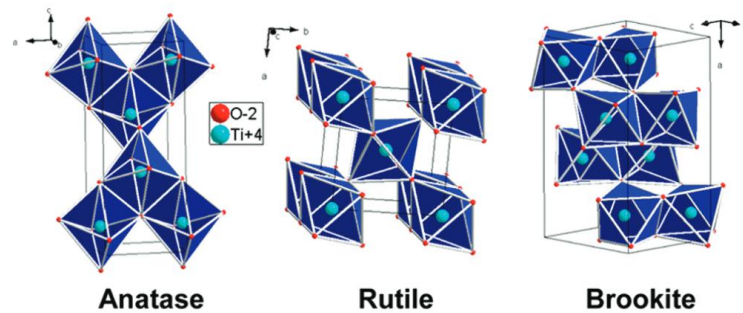


Figure 2.1: Crystallographic structures of anatase (tetragonal), rutile (tetragonal), and brookite (orthorhombic). Reprinted with permission from Ref.¹⁸

TiO_2 is a semiconductor having a conduction band (CB) and a valence band (VB) which are separated by the bandgap energy (E_{BG}). Herein, the occupied VB consists mainly of 2p orbitals from O^{2-} , while the VB mostly contains of 3d orbitals from Ti^{IV} . The E_{BG} of the different TiO_2 polymorphs vary from each other due to their different unit cell structures. The E_{BG} of anatase is 3.2 eV¹⁹, of rutile 3.0 eV²⁰ and of brookite between 3.0 eV and 3.4 eV²¹.

Photocatalysis utilizes the property of semiconductors to absorb photon energy due to their E_{BG} . In this regard, the semiconductor catalyzes oxidation and reduction reactions

2 Theoretical background

upon light illumination with energy higher or equal to the E_{BG} . TiO_2 is the most widely used photocatalyst for air and water purification, because of its stability over a wide pH range, its abundance, and its nontoxicity.²² When TiO_2 is exposed to UV illumination ($\lambda < 390$ nm) an electron is excited from the valence band to the conduction band leaving an electron vacancy also referred to as a hole in the VB.



About 90 % or more of the photogenerated charge carriers recombine within 10 ns, emitting thermal or photon energy.²³ The remaining electrons and holes migrate from the bulk to the photocatalyst surface, where electrons are trapped at Ti^{III} centers and holes at $O_s^{\bullet-}$.



The trapped charge carriers either recombine or react with species adsorbed on the TiO_2 surface (see Figure 2.2).

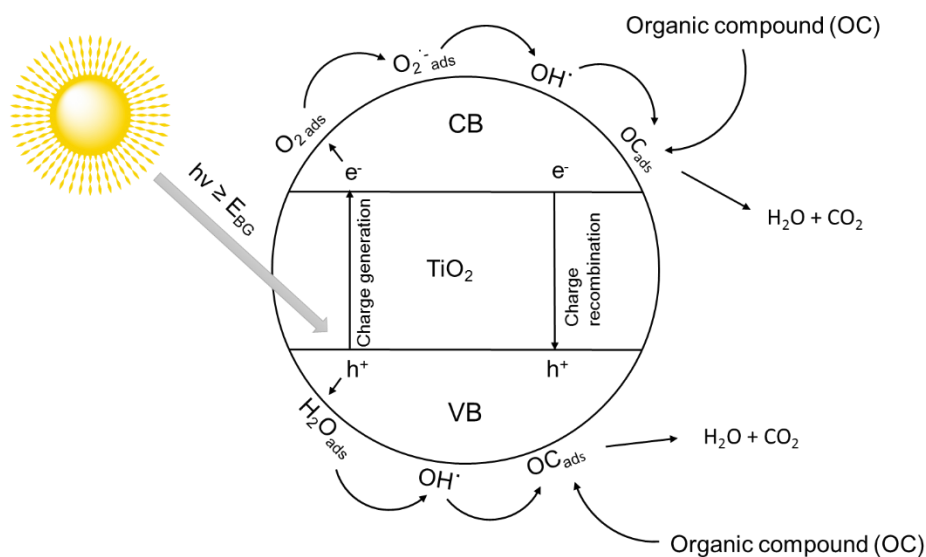


Figure 2.2: Schematic illustration of the photocatalytic degradation process on the TiO_2 surface.

The high redox potential of 2.7 V (vs. NHE) of the holes in TiO_2 allows the oxidation most of the organic compounds yielding CO_2 and H_2O as reaction products.²⁴ Besides the direct oxidation the organic compounds can also be oxidized by hydroxyl radicals, which are formed by oxidation of water molecules through holes.



The electrons have a potential of -0.5 V (vs. NHE), being less reactive compared to the holes.²⁴ They most likely reduce molecular O₂ to form a superoxide radical anion (-0.33 V vs. NHE).²⁵ These species can further be protonated forming firstly HO₂[•] radicals and afterwards hydrogen peroxide.



Hydrogen peroxide can be further reduced by electrons forming hydroxyl radicals, which can finally oxidize organic compounds present on the TiO₂ surface.



The role and the importance of each of these reaction steps for the photocatalytic degradation of organic compounds has not been completely understood yet. OH[•] radicals are recognized as primary species in the photooxidation of organic compounds. Furthermore, molecular O₂ can also be involved in photocatalytic oxidation reactions resulting in the formation of various intermediates, which are finally decomposed into CO₂ and H₂O in a sequence of reaction steps.²⁶ Hence, the photocatalytic degradation of organic compounds is a highly complex process.

2.2 Surface structure of TiO₂

Photocatalytic degradation reactions occur on the TiO₂ surface. Therefore, it is of utmost importance to understand the surface structure of TiO₂. Two kinds of oxygen species exist on the TiO₂ surface: terminal oxygen atoms, that are one fold coordinated to Ti and bridging oxygen atoms, which are two-fold coordinated to Ti (see Figure 2.3).^{15,27,28} The terminal oxygen atoms are removed from the surface by heating up to 623 K, while the bridging oxygen atoms remain stable up to 773 K.^{28,29} When water molecules are adsorbed on the TiO₂ surface, an oxygen exchange can occur between the terminal OH from TiO₂ and adsorbed water. In contrast, the bridging oxygen atoms are not affected by the presence of adsorbed water.³⁰

2 Theoretical background

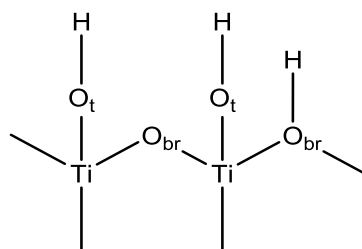


Figure 2.3: Schematic illustration of the two oxygen species located on the TiO₂ surface.

Water is one of the most important adsorbates on the TiO₂ surface. At ambient conditions water vapor interacts with the TiO₂ surface and affects the adsorption and reaction properties of TiO₂. Nosaka *et al.*³¹ studied the water adsorption on the TiO₂ surface by ¹H-NMR. The spectra showed the presence of three water layer species on the TiO₂ surface, when the sample was exposed to air (see Figure 2.4). The mobility of the water molecules within these layers increases in the order of III < II < I. Water layer I is weakly adsorbed and is located at the outermost layer of the TiO₂ surface, while water layer II shows less mobility and is located in the inner layer. Water layer III is very rigid with restricted mobility and is located near the solid surface. It also includes chemically bound OH groups.

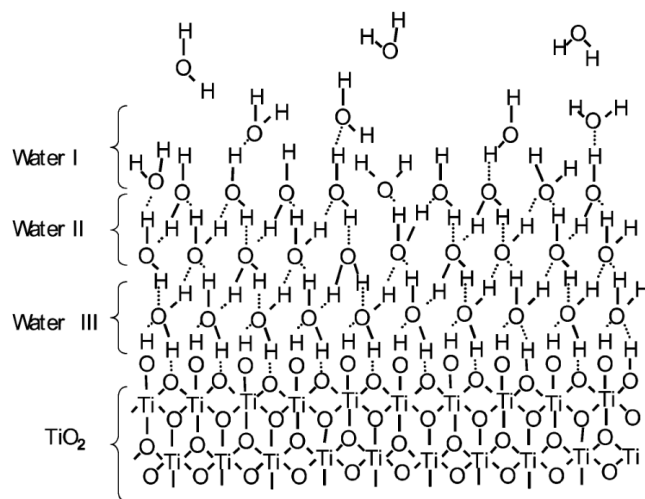


Figure 2.4: Proposed structure of water layers on the TiO₂ surface in the dark. Reprinted with permission from Ref.³¹

2.3 Acetaldehyde in the dark

One example of an organic compound that can be degraded in the presence of TiO₂ is the air pollutant acetaldehyde. Acetaldehyde is proposed to be molecularly adsorbed on the TiO₂ surface in two forms as illustrated in Figure 2.5. Either hydrogen bridge bonds are

formed between the carbonyl group of acetaldehyde and the surface hydroxyl groups from the TiO_2 surface or acetaldehyde is adsorbed in a more stable way through its oxygen lone pair with Ti^{IV} sites of TiO_2 .³²

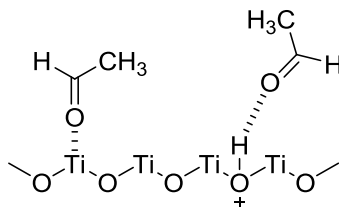


Figure 2.5: Acetaldehyde adsorption on the TiO_2 surface in the dark.

When two acetaldehyde molecules are adsorbed on the TiO_2 surface, they react *via* an aldol condensation forming crotonaldehyde, which is catalyzed by the TiO_2 surface (see Figure 2.6). The reaction proceeds with ketones and aldehydes having a hydrogen atom on the α -carbon. Thus, formaldehyde is not suitable for this reaction, while for example acetone molecules form mesityl oxide on the TiO_2 surface.³³ The aldol condensation of acetaldehyde does not only take place on TiO_2 surfaces, but also on other metal oxides such as CeO_2 ,⁸ ZrO_2 , MgO ,³⁴ and Al_2O_3 .³⁵ In the absence of a metal oxide, the reaction usually proceeds in acidic or basic media. Idriss *et al.*⁷ and Singh *et al.*³⁶ investigated the aldol condensation of acetaldehyde molecules on the TiO_2 surface. These authors proposed that a lattice oxygen atom from the TiO_2 surface acts as a base abstracting one proton from an α -carbon of an adsorbed acetaldehyde molecule forming a surface hydroxyl OH species and a $^-\text{CH}_2\text{CHO}$ (step 1 and 2). Subsequently, the nucleophilic carbon species $^-\text{CH}_2\text{CHO}$ attacks the electrophilic carbonyl group of a second adsorbed acetaldehyde molecule, which in turn abstracts the proton from the hydroxyl group, yielding 3-hydroxybutanal (step 3). Upon dehydration crotonaldehyde is finally generated (step 4), which is adsorbed on the TiO_2 surface at Ti^{IV} sites. The formation of crotonaldehyde is facilitated on oxidized surfaces, because a higher number of surface oxide anions is available to initiate the reaction by abstracting a proton from acetaldehyde.⁷ On TiO_2 -supported Pt, Rh, and Au catalysts the formation of crotonaldehyde has also been observed. Herein, crotonaldehyde is adsorbed in two different ways, it either interacts through its oxygen lone pair with Ti^{IV} sites of TiO_2 or it is adsorbed on metallic sites through its carbon atom from the aldehyde group.³⁷

2 Theoretical background

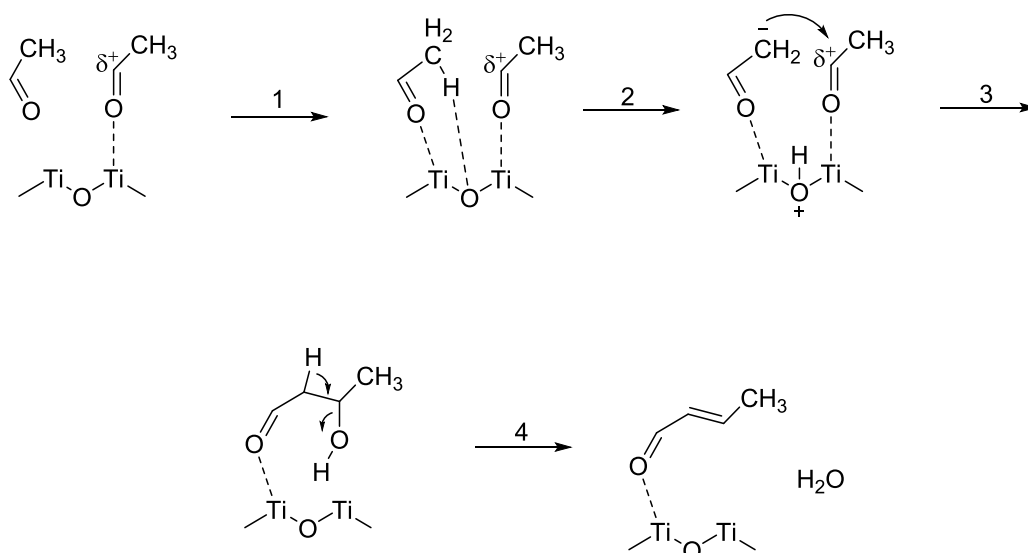


Figure 2.6: Proposed reaction mechanism for the aldol condensation of two acetaldehyde molecules, forming crotonaldehyde and water on the TiO₂ surface in the dark.

In many applications the formation of species with higher masses as the educt is undesired. In this sense the evolution of crotonaldehyde can also be suppressed by a SO₄²⁻ modification of the TiO₂ surface. Herein, the initial step of proton abstraction from acetaldehyde is inhibited due to an interaction between the H-atom of the α-carbon of acetaldehyde and an oxygen from the sulfate group (see Figure 2.7).³⁸

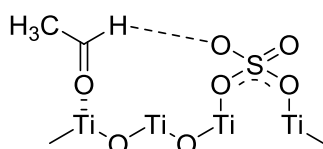


Figure 2.7: Schematic illustration of an acetaldehyde molecule adsorbed on the SO₄-TiO₂ surface.

2.4 Acetaldehyde upon UV illumination

Upon UV illumination acetaldehyde is degraded over TiO₂. A few studies have been published on the degradation mechanism of gaseous acetaldehyde.^{11,38–40} Since acetaldehyde is also an intermediate of the photooxidation of ethanol these results are also included here.^{10,41–43} The oxidation of aldehydes in the presence of molecular O₂ proceeds *via* radical chain reactions on the TiO₂ surface (see Figure 2.8 to Figure 2.11). The initial step involves an abstraction of a hydrogen atom from the α-carbon of acetaldehyde by an OH[•] forming a CH₃C[•]O radical (step 1). Subsequently, O₂ attacks the radical producing an unstable peroxy radical (step 2), which further reacts with two acetaldehyde molecules forming two acetic acid molecules (step 3 and 4).

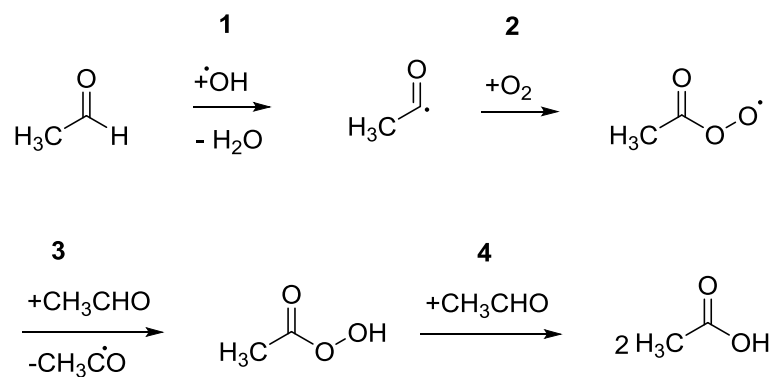


Figure 2.8: Proposed photocatalytic degradation mechanism of acetaldehyde forming acetate over TiO_2 in the presence of O_2 .

The methyl radical $\text{CH}_3\cdot$ is generated *via* two reaction pathways shown in Figure 2.9. Either an $\text{OH}\cdot$ abstracts one hydrogen atom from acetic acid forming an acetate radical, which decomposes into CO_2 and $\text{CH}_3\cdot$ *via* a photo-Kolbe reaction pathway or a dimerization of two peroxy radicals produced in step 2 of Figure 2.8 occurs decomposing then into CO_2 , O_2 and $\text{CH}_3\cdot$. Ohko *et al.*¹¹ proposed that under weak UV illumination the methyl radical is generated *via* the second pathway, while with increasing UV intensity the first pathway becomes the predominant one.

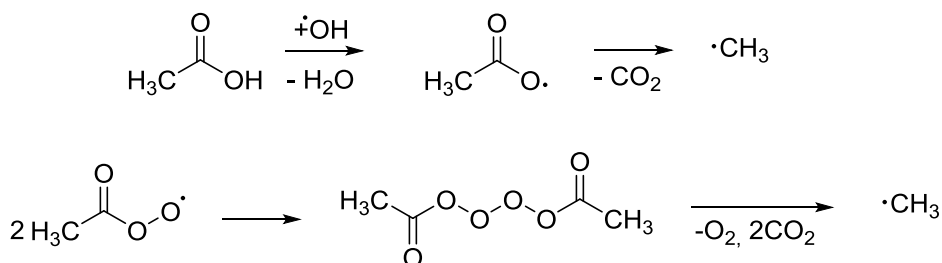


Figure 2.9: Proposed reaction mechanisms for the formation of the methyl radical during acetaldehyde degradation over TiO_2 in the presence of O_2 .

As illustrated in Figure 2.10 for the formation of formaldehyde the methyl radical is attacked by O_2 forming a methyl peroxy radical, which subsequently reacts with the peroxy radical generated in step 2 of Figure 2.8. In the following step formaldehyde, acetic acid and O_2 are evolved.

2 Theoretical background

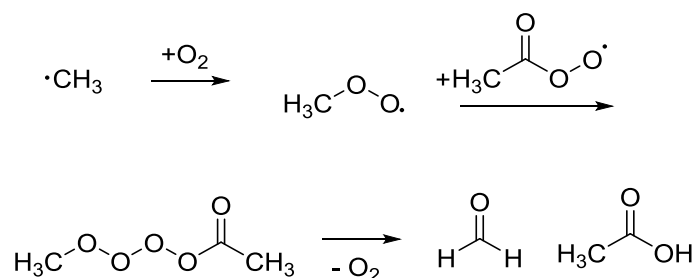


Figure 2.10: Formation of formaldehyde and acetic acid during the photooxidation of acetaldehyde over TiO_2 in the presence of O_2 .

In the final step $\text{OH}\cdot$ abstracts again one hydrogen atom from formaldehyde forming $\text{HCO}\cdot$, which subsequently reacts with another $\text{OH}\cdot$ generating formic acid that is oxidized yielding CO_2 (see Figure 2.11).⁴⁴⁻⁴⁶

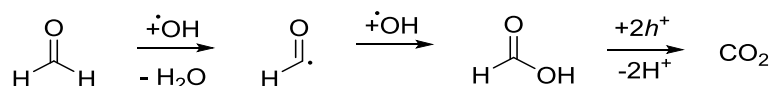


Figure 2.11: Formation of formic acid and CO_2 during the photooxidation of acetaldehyde over TiO_2 in the presence of O_2 .

2.5 Role of lattice oxygen atoms in photocatalytic reactions

In addition to the involvement of $\text{OH}\cdot$ and O_2 in oxidation reactions, lattice oxygen atoms from the TiO_2 surface can also participate in photocatalytic reactions. One example is the photoinduced oxygen isotopic exchange (POIE) occurring between O_2 and bridging oxygen atoms from the TiO_2 lattice upon UV illumination.⁴⁷ A proposed reaction mechanism involving Ti^{16}O_2 and $^{18}\text{O}_2$ is shown in Figure 2.12.⁴⁸ Upon UV illumination the photogenerated holes are trapped as $^{16}\text{O}_{\text{br}}\cdot^-$, while the electrons are trapped at neighboring Ti^{III} sites inducing a Ti-O bond breakage. The electron at the Ti^{III} is transferred to the $^{18}\text{O}_2$ and simultaneously an $^{18}\text{O}_2\text{-Ti}^{\text{IV}}$ bond is formed, which induces a weakening of the $^{18}\text{O}\text{-}^{18}\text{O}$ bond. By a further electron transfer to the superoxide anion, the $^{18}\text{O}\text{-}^{18}\text{O}$ bond breaks resulting in the formation of $^{18}\text{O}^{2-}$, Ti^{IV} and $(^{18}\text{O}\text{-}^{16}\text{O})_{\text{br}}\cdot^-$. The final step involves the trapping of a further hole at $(^{18}\text{O}\text{-}^{16}\text{O})_{\text{br}}\cdot^-$ inducing an abstraction of the $^{18}\text{O}^{16}\text{O}$ into the gas phase. The remaining oxygen vacancy V_{o} is filled with the $^{18}\text{O}^{2-}$.

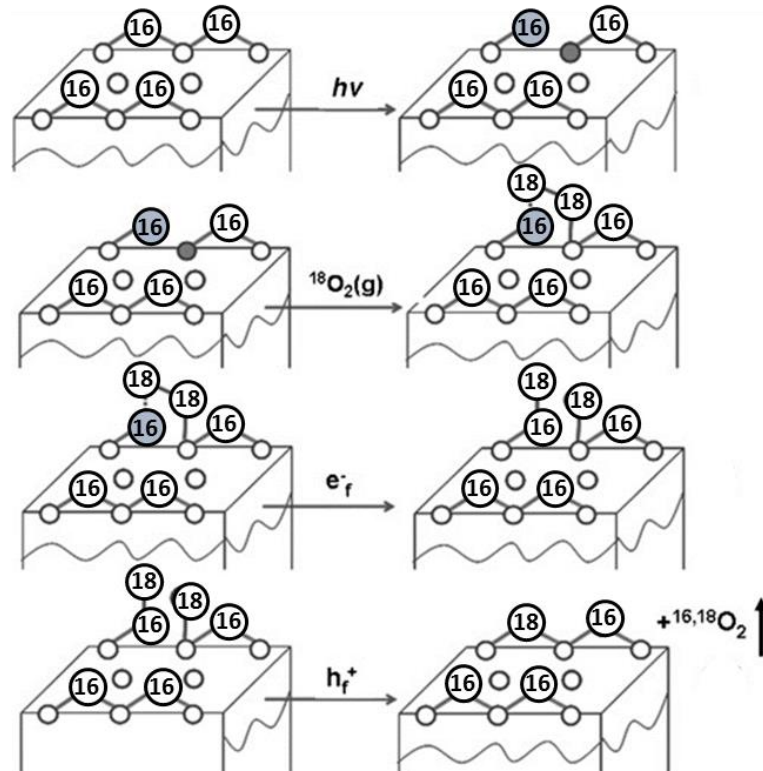


Figure 2.12: Proposed mechanism for the photoinduced oxygen isotopic exchange between $^{18}\text{O}_2$ and Ti^{16}O_2 upon UV illumination and in the absence of H_2O . Large white circle: bridging oxygen ion; large grey circle: bridging oxygen radical; small white circle: Ti^{IV} ion, small grey circle: Ti^{III} ion. Adapted from Ref ⁴⁸.

Besides the POIE between lattice oxygen atoms and molecular O_2 , bridging oxygen atoms can also be involved in oxidation reactions. By ATR-FTIR spectroscopy it has been shown that the oxidation of cyclohexane proceeds *via* the Mars-van Krevelen mechanism.⁴⁹ This mechanism describes an oxidation reaction occurring on transition metal oxide surfaces.⁵⁰ Herein, the gaseous molecule A_g is firstly adsorbed as A_{ads} on the transition metal oxide surface, where it reacts with a lattice oxygen atom ($\text{O}_{\text{lattice}}$) from the surface forming AO_{ads} . The product AO_g is then desorbed from the surface leaving an oxygen vacancy, which is replenished by an oxygen atom supplied from adsorbed O_2 .



2 Theoretical background

A schematic illustration of the oxidation mechanism of cyclohexane over TiO_2 is shown in Figure 2.13. Upon UV illumination the adsorbed cyclohexane is oxidized into cyclohexanone by an incorporation of a lattice oxygen atom ^{16}O from the TiO_2 surface. The remaining oxygen vacancy is replenished by an oxygen atom supplied from $^{18}\text{O}_2$.

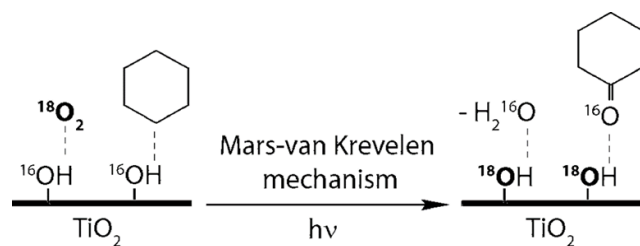


Figure 2.13: Proposed reaction mechanism for the photooxidation of cyclohexane into cyclohexanone proceeding *via* the Mars-van Krevelen mechanism. Reprinted with permission from Ref.⁴⁹

3 Materials and experimental methods

3.1 Materials

Hombikat UV-100 containing 100 % anatase was provided by Sachtleben Chemie GmbH. Acetaldehyde gas containing 251 ppm in N₂ and carbon dioxide containing 1 % CO₂ in argon were supplied from Linde Gas AG. Ti¹⁸O₂ synthesized according to the reported procedure, was kindly provided by Juan Montoya.¹⁵

3.2 Experimental methods

3.2.1 Specific surface area measurements

The specific surface area of solid materials can be determined using the Brunauer-Emmet-Teller (BET) theory.⁵¹ For this purpose, a gas mixture of 30 % N₂ and 70 % He is directed over the sample at 77 K. When the gas is adsorbed on the surface a change in the gas pressure occurs, which can be measured. After adsorption the temperature is increased again inducing a desorption of the gas molecules from the surface and thus a change in the gas pressure that can be determined again. From the resulting adsorption and desorption isotherms the specific surface area is calculated. In this study, the specific surface area measurements were carried out employing a FlowSorb II 2300 instrument (Micromeritics, USA).

3.2.2 Raman spectroscopy

For the (ambient temperature and depolarized) Raman measurements a confocal Bruker Senterra micro-Raman spectrometer equipped with an Olympus BX 51 microscope was used. A 532 nm laser with a power of 2 mW was employed as excitation source. The instrument precision was within $\pm 3 \text{ cm}^{-1}$.

3.2.3 X-ray diffraction

The TiO₂ samples were characterized by X-ray diffraction (XRD) using Cu K α radiation ($\lambda = 0.154178 \text{ nm}$) with a Bruker D8 Advanced Diffractometer. The patterns were recorded in the 2θ range between 5° and 110° in steps of 0.011° and with a step time of 0.7 s. The crystalline mean size is determined by the Scherrer equation:

$$\tau = \frac{K \times \lambda}{\beta \times \cos(\theta)} \quad (11)$$

3 Materials and experimental methods

τ is the mean size of the crystalline domains, K is a dimensionless shape factor of 0.9, λ is the X-ray wavelength, β is the line broadening at half of the maximum intensity and Θ is the Bragg angle.

The amount of the crystalline components in a powder can be calculated by the Rietveld refinement. The Rietveld refinement was carried out using the Bruker DIFFRACplus TOPAS V4.2 software (Bruker AXS Inc., Madison, Wisconsin, USA). The space groups $I4_1/amd$ and $P4_2/mnm$ were assumed for anatase and rutile, respectively, as starting points for the refinement. The scale factors, lattice parameters, positional parameters, and the phase abundance were optimized during the refinements. The instrumental parameters were determined with a LaB6 sample (Sigma Aldrich).

3.2.4 Field-emission scanning electron microscopy

The field-emission scanning electron microscopy (FE-SEM) measurements were carried out on a JEOL JSM-6700F with an acceleration voltage of 2 kV. The SEM images were provided by a secondary electron detector and a magnification of 50000 times.

3.2.5 Attenuated total reflection Fourier-transform infrared spectroscopy

In situ attenuated total reflection Fourier-transform infrared (ATR-FTIR) spectroscopy is an established technique providing information about the interfacial processes occurring on the TiO₂ surface. The adsorption of molecules, either from the gas or the liquid phase on the TiO₂ surface can be investigated, as well as the intermediates and products formed during the photocatalytic degradation process. Therefore, ATR-FTIR spectroscopy is an ideal method to gain a deeper understanding of the photocatalytic processes on the TiO₂ surface.

ATR-FTIR spectroscopy is based on a combination of an internal reflection element (IRE) with a FTIR spectrometer. In IR spectroscopy molecules with an electric dipole moment are excited from the ground vibrational state to a higher level of energy by absorption of IR light. In this context, the absorption energy is characteristic for specific molecular groups and provides information about the molecular structure and molecular interactions. The IRE is a material with a relatively high refractive index, thus when IR radiation enters the medium a total reflection occurs according to the Snell's law. In the 1960s Harrick⁵² and Fahrenfort⁵³ coupled, independently from each other, an IRE with an IR spectrometer. For this purpose, the sample was deposited on the IRE in order to achieve a direct contact between the sample and the IRE. The IRE or ATR crystal usually

has a higher refractive index (n_1) compared to the sample (n_2). Thus, when an IR beam is directed onto the edge of an ATR crystal, the IR light is totally reflected several times through the crystal until it enters the detector, where an IR spectrum is recorded (see Figure 3.1). An important parameter of the total reflection is the incidence angle θ , which is dependent on the refractive indices of the IRE (n_1) and the sample (n_2) shown in the equation below:

$$\theta = \sin^{-1}\left(\frac{n_2}{n_1}\right) \quad (12)$$

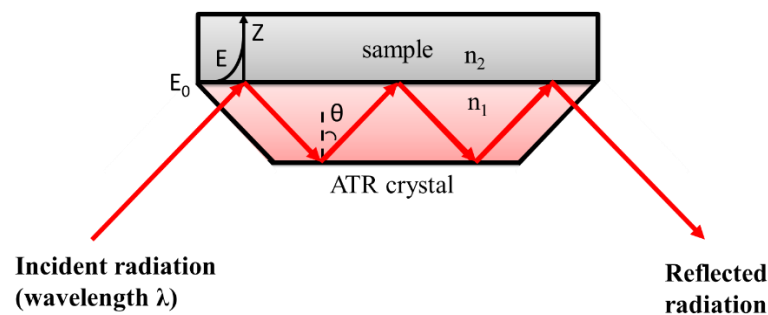


Figure 3.1: Schematic illustration of the ATR-FTIR unit.

The internal reflectance creates an evanescent field, which decays exponentially in the less dense medium according to equation 13:

$$E = E_0 \exp \left[-\frac{2\pi n_1}{\lambda} \left(\sin^2 \theta - \left(\frac{n_2}{n_1} \right)^2 \right)^{1/2} Z \right] \quad (13)$$

E is the amplitude in the sample at the depth Z , E_0 is the amplitude at the sample surface, where Z is 0 and λ is the wavelength of the IR beam. The distance where the amplitude decays to a value of \exp^{-1} of its value at the sample surface is defined as the penetration depth (d_p).

$$d_p = \frac{\lambda}{2\pi n_1} \left(\sin^2 \theta - \left(\frac{n_2}{n_1} \right)^2 \right)^{-1/2} \quad (14)$$

When the evanescent wave enters the sample distinct energy is extracted, which can be detected. The penetration depth can vary from 0.5 to 5 μm and is dependent on the wavelength of the IR beam (see equation 14). At higher wavelengths the depth of

3 Materials and experimental methods

penetration is enhanced, therefore the signal of the ATR spectrum is also increased compared to lower wavelengths.

In the present study, a zinc selenide (ZnSe, Pike Technologies) crystal with a surface of 6.8×72 mm and a refractive index of 2.4 was used for the analyses in the mid IR region, that is in the wavenumber range between 800 and 4000 cm^{-1} . The IR beam has an incidence angle of 45° and is 9 times totally reflected at the upper face of the ZnSe crystal.

The FTIR spectrometer employed was a Bruker IFS 66 equipped with a deuterated triglycine sulfate (DTGS) detector. The interferometer and the infrared light path in the spectrometer were constantly purged with argon, in order to avoid CO_2 and H_2O contamination. Each spectrum was an average of 300 scans with a resolution of 4 cm^{-1} . Before each experiment, a sequence of blank spectra of the TiO_2 film for 2 h in the dark and for 6 h upon UV illumination in the absence of acetaldehyde were recorded. After the blank spectra, acetaldehyde was directed over the same film and spectra were recorded in the dark (2 h) and upon UV illumination (6 h). The final spectra were obtained by subtracting the blanks from the ones in the presence of acetaldehyde. For experiments under humidity (58 %), O_2 was directed through a washing flask to generate a humidified gas flow. A LED lamp (LED Flächenstrahler) was used as UV illumination source, which was supplied by OMICRON with a maximum emission wavelength of 365 nm and an intensity of 1 mW cm^{-2} . The gas flow was set to 100 mL min^{-1} with an acetaldehyde concentration of 63 ppm (SIERRA[®]). A closed compartment made of Plexi-Glass[®] (PMMA, Polymethylmethacrylate) was built and attached to the upper part of the ZnSe crystal in order to generate a continuous gas flow (see Figure 3.2).

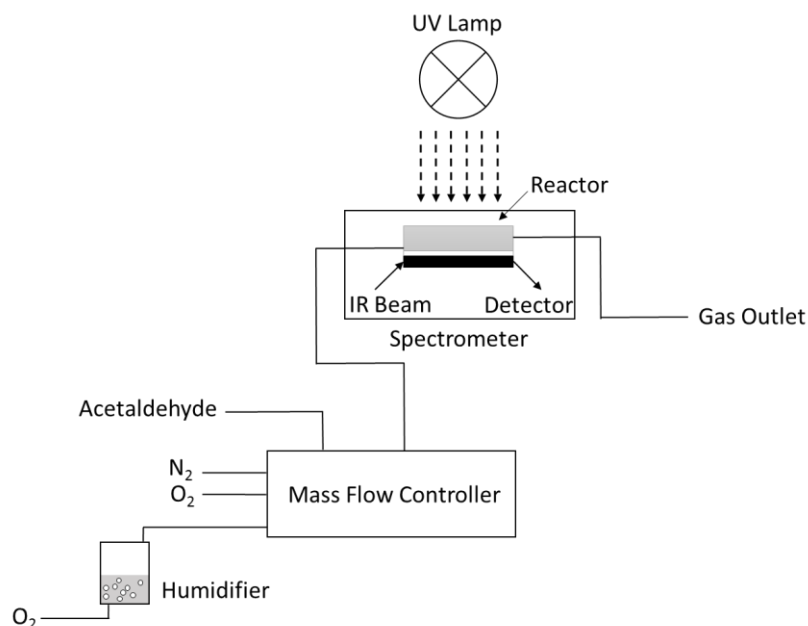


Figure 3.2: Experimental set up for the ATR-FTIR measurement. Reprinted from Ref.¹²

3.2.6 Gas chromatography / photoionization detector

The acetaldehyde concentration in the gas phase was constantly detected by gas chromatography coupled with a photoionization detector (GC/PID). The experimental set up to monitor the concentration of acetaldehyde as a function of time is shown in Figure 3.3. After directing 1 ppm of acetaldehyde in N₂/O₂ atmosphere over the TiO₂ film, the concentration of acetaldehyde at the reactor outlet was determined every 5 min by a GC/PID (SYNTECH Spectras GC 955). The total gas flow was set to 1 L min⁻¹ by mass flow controllers (Brooks instruments). A humidified gas flow of 50 % was generated by directing O₂ gas through a washing flask and afterwards passing it over the sample. The reactor was made of PMMA with a transparent borosilicate glass plate attached on the upper part. The concentration of acetaldehyde was monitored for 2.5 h in the dark and for 6 h upon UV illumination. The light source used was a Philips CLEO compact fluorescent tube with an emission wavelength of $\lambda_{\text{max}} = 365 \text{ nm}$ and an intensity of 1 mW cm⁻².

3 Materials and experimental methods

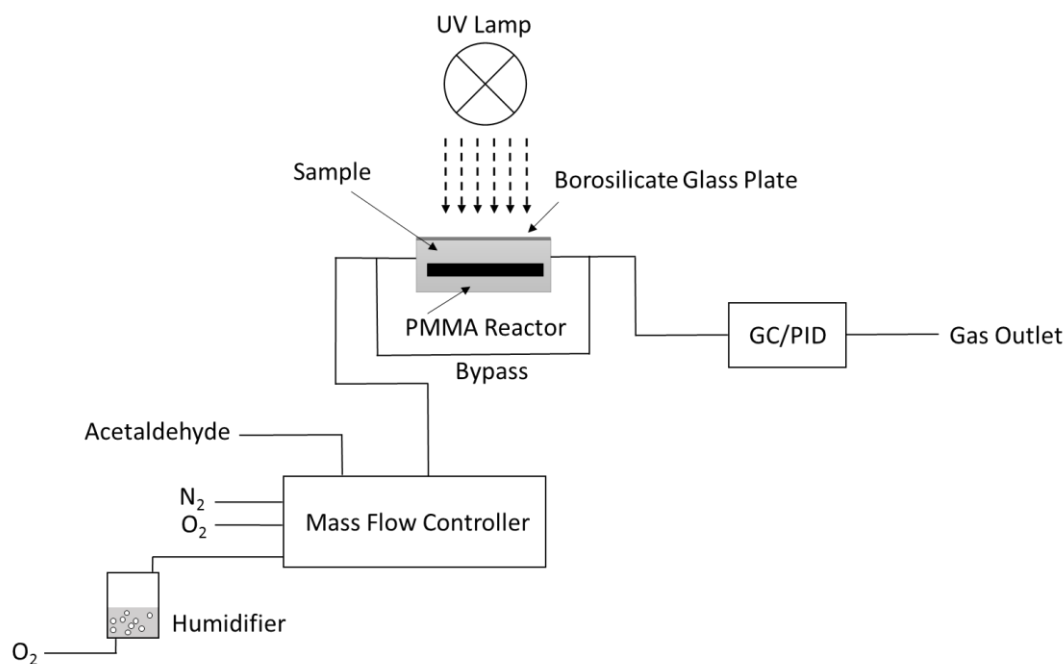


Figure 3.3: Experimental set up to monitor the concentration of acetaldehyde as a function of the time during acetaldehyde treatment over TiO₂. Reprinted from Ref.¹²

3.2.7 Mass spectrometry

Besides the detection of acetaldehyde in the gas phase by GC/PID, mass spectrometry (MS) was used to detect gaseous products formed in the dark and upon UV illumination. The employed experimental set up is shown in Figure 3.4. The prepared TiO₂ film in the PMMA holder was placed in a reactor made of PMMA with a transparent borosilicate glass plate attached on the upper part. A gas flow of 75 mL min⁻¹ (SIERRA[®]) with a concentration of 50 ppm of acetaldehyde in N₂ was directed over the TiO₂ film and the gas at the reactor outlet was constantly analysed by a quadrupole mass spectrometer (Hiden HPR-20). For the measurements an UV-100 film was treated with acetaldehyde for 2 h in the dark and for 6 h upon UV illumination. A LED lamp (LED Flächenstrahler) was used as UV illumination source, which was supplied by OMICRON having a maximum emission wavelength of 365 nm and an intensity of 1 mW cm⁻². For the isotopic studies the Ti¹⁶O₂ and Ti¹⁸O₂ films were treated with 50 ppm of acetaldehyde for 1.5 h in the dark and for 3 h upon UV illumination. The gas flow was set to 10 mL min⁻¹ (SIERRA[®]). The light source used was a Philips CLEO compact fluorescent tube with an emission wavelength of $\lambda_{\text{max}} = 365$ nm and an intensity of 1 mW cm⁻².

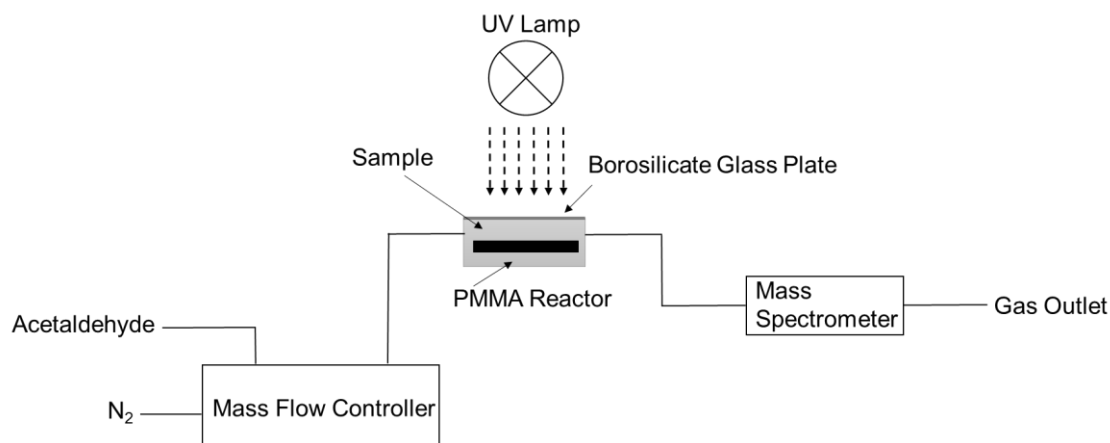


Figure 3.4: Experimental set up to detect the evolution of gaseous products during acetaldehyde degradation over TiO₂ upon UV illumination. Reprinted from Ref.¹²

3.2.8 TiO₂ film preparation

For the ATR-FTIR measurements 5.75 g L⁻¹ of a TiO₂ suspension was prepared in deionized water and was dispersed for 15 min in an ultrasonic bath. Afterwards an aliquot of 400 μl was placed on the ZnSe crystal, which was gently balanced, in order to distribute the aliquot equally. After evaporation of the water, a homogenous film was obtained, which had a coverage of 2.3 g m⁻² and a film thickness of 1.7 ± 0.3 μm according to Hug and Sulzberger.⁵⁴

For the gas analyses using GC/PID the TiO₂ powder was pressed into a PMMA holder with an average size of 4.3 × 4.3 cm. The resulting pellet had a surface size of 18.49 cm² and was pre-illuminated by UV light (365 nm, 1 mW cm⁻², Philips CLEO 100W-R) for at least 24 h, in order to eliminate organic residues from the surface.

For the MS analysis 5.75 g L⁻¹ of a TiO₂ suspension was prepared in deionized water and was dispersed for 15 min in an ultrasonic bath. Afterwards 4 ml were placed on a PMMA holder with a size of 4.3 × 9.2 cm. The holder was gently balanced, in order to distribute the aliquot equally. After evaporation of the water, a homogenous film was obtained.

3 Materials and experimental methods

4 Results

4.1 Characterization of the TiO₂ powders

4.1.1 Raman spectroscopy

The UV-100 (Ti¹⁶O₂) powder and the synthesized isotope-labeled Ti¹⁸O₂ were characterized by Raman spectroscopy. The corresponding spectra and mode assignment are illustrated in Figure 4.1 and in Table 4.1. Ti¹⁶O₂ exhibits peaks at 144, 197, 397, 516, and 640 cm⁻¹, which can be assigned to the Raman vibration modes of E_g (1), E_g (2), B_{1g} (1), B_{1g} (2) + A_{1g}, and E_g (3), respectively. In contrast, the peaks E_g (2), B_{1g} (2) + A_{1g}, and E_g (3) of the labeled Ti¹⁸O₂ are red-shifted by 11, 27 and 36 cm⁻¹, respectively, indicating an ¹⁸O purity in Ti¹⁸O₂ of 97 %.^{55,56}

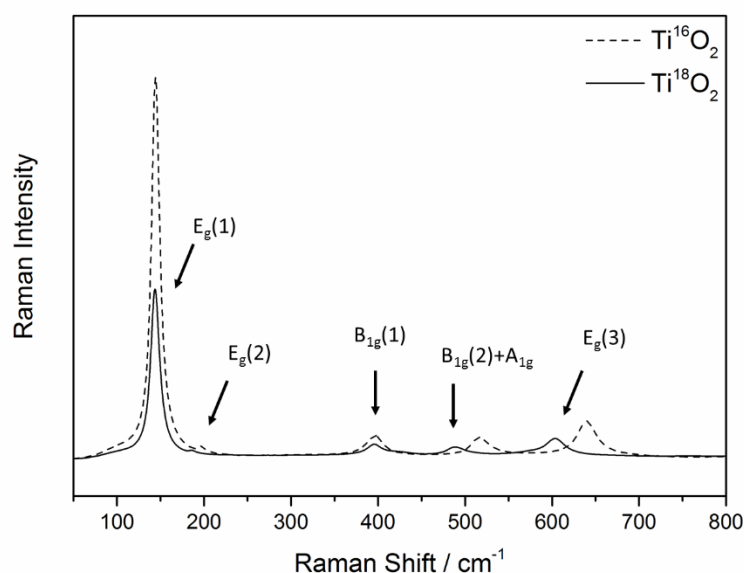


Figure 4.1: Raman spectra of Ti¹⁶O₂ (UV-100) and Ti¹⁸O₂. Reprinted with permission from Ref.⁵⁷

Table 4.1: Raman vibrations and the corresponding mode assignments of Ti¹⁶O₂ and Ti¹⁸O₂.

	UV-100 / Ti ¹⁶ O ₂	Ti ¹⁸ O ₂
E _g (1)	144 cm ⁻¹	144 cm ⁻¹
E _g (2)	197 cm ⁻¹	186 cm ⁻¹
B _{1g} (1)	397 cm ⁻¹	396 cm ⁻¹
B _{1g} (2) + A _{1g}	516 cm ⁻¹	489 cm ⁻¹
E _g (3)	640 cm ⁻¹	604 cm ⁻¹

4 Results

4.1.2 X-ray diffraction

The XRD patterns of Ti^{16}O_2 and Ti^{18}O_2 are illustrated in Figure 4.2. Both samples exhibit peaks at 25, 38, 48, 54, and 63° corresponding to the (101), (004), (200), (211), and (213) planes of tetragonal anatase. Furthermore, the isotope-labeled Ti^{18}O_2 shows additional peaks at 28 and 36° which are referred to the (110) and (101) planes of tetragonal rutile. According to the calculations of the Rietveld refinement the Ti^{18}O_2 consists of 89.9 % anatase and 10.1 % rutile. The anatase particle size is 7.05 nm for UV-100 and 17.77 nm for Ti^{18}O_2 according to the Scherrer equation.

The BET surface area of UV-100 is 280 $\text{m}^2 \text{g}^{-1}$ and of Ti^{18}O_2 is 32 $\text{m}^2 \text{g}^{-1}$.¹⁵

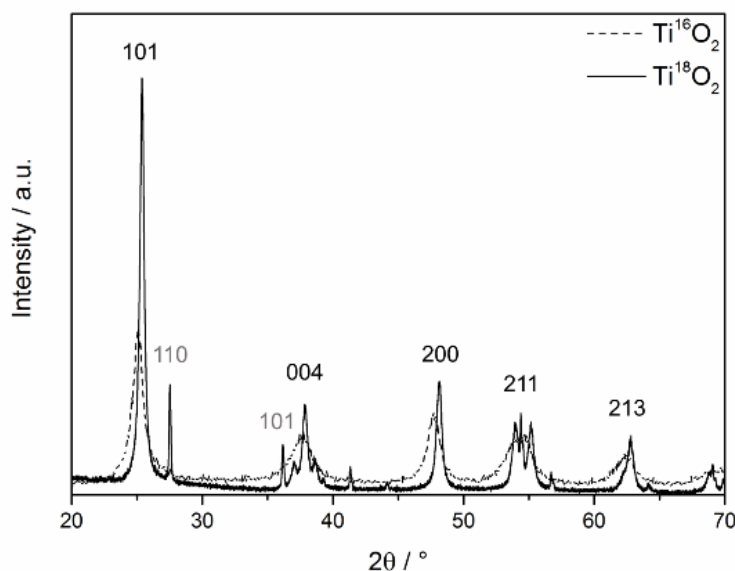


Figure 4.2: XRD patterns of Ti^{16}O_2 and Ti^{18}O_2 . Reprinted with permission from Ref.⁵⁷

4.1.3 Scanning electron microscopy

Figure 4.3 illustrates the SEM images of UV-100 and Ti^{18}O_2 . Both samples contain particles with spherical shape that form agglomerates. The particle size of UV-100 (7.05 nm) and Ti^{18}O_2 (17.77 nm) calculated by the Scherrer equation corresponds well with the SEM images.

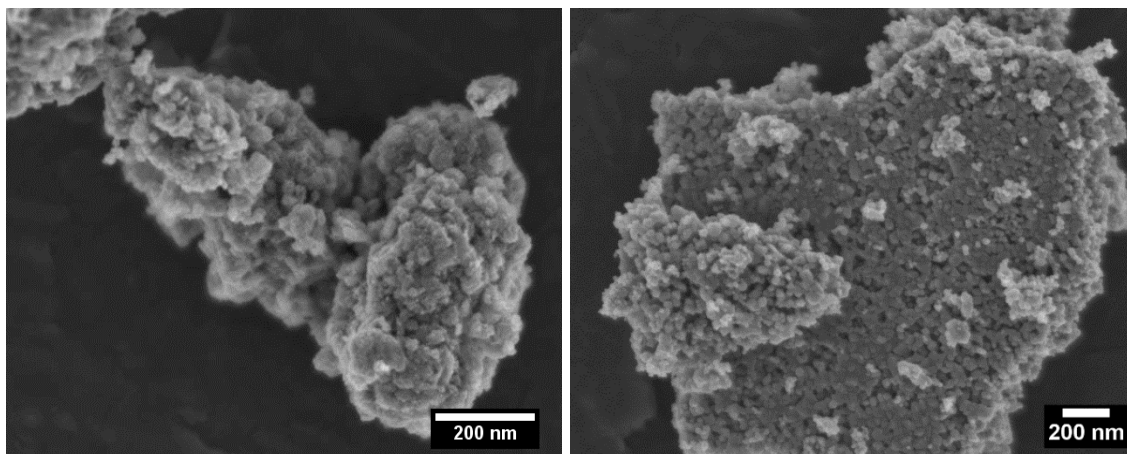


Figure 4.3: SEM images of UV-100 (left) and Ti^{18}O_2 (right).

4.2 Acetaldehyde adsorption and crotonaldehyde formation on the TiO_2 surface in the dark

As shown in Figure 4.4, when an UV-100 film is treated with 1100 ppb of acetaldehyde in the presence of O_2 under dry conditions in the dark, the concentration of acetaldehyde detected at the reactor outlet decreases from 1100 ppb to 700 ppb and remains then constantly low. Interestingly, the concentration does not increase to the initial value again even after 12 h of acetaldehyde treatment (see Figure 4.5).

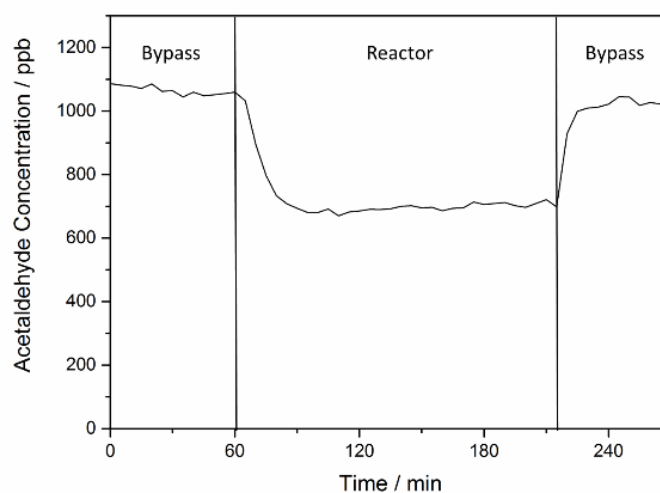


Figure 4.4: Time evolution of the acetaldehyde concentration detected at the reactor outlet in the presence of O_2 under dry conditions in the dark. During the first 60 min the acetaldehyde concentration is kept constant at 1100 ppb in the bypass mode. Afterwards the gas mixture is directed over an UV-100 for 2.5 h using the reactor mode, before it is turned back to the bypass mode again. Reprinted from Ref.¹²

4 Results

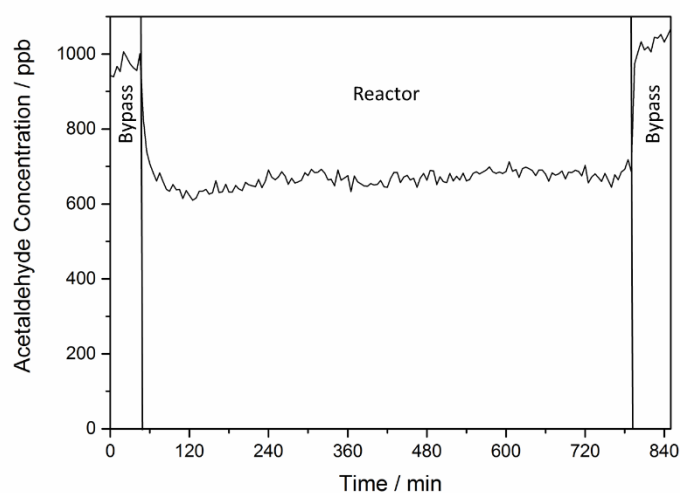


Figure 4.5: Time evolution of the acetaldehyde concentration in O_2 atmosphere detected at the reactor outlet under dry conditions in the dark. During the first 50 min the acetaldehyde concentration is kept constant at 1000 ppb in the bypass mode. Afterwards the gas mixture is directed over an UV-100 for 12 h using the reactor mode, before it is turned back to the bypass mode again. Reprinted from Ref.¹²

ATR-FTIR analyses of an UV-100 film treated with gaseous acetaldehyde were performed, in order to identify the reason for the constantly decreased acetaldehyde concentration in the dark. For this purpose, *in situ* ATR-FTIR spectra of an UV-100 film were recorded during acetaldehyde treatment under dry conditions in O_2 atmosphere for 2 h in the dark. Figure 4.6 illustrates the ATR-FTIR spectra in the wavenumber range between 1000 cm^{-1} and 1800 cm^{-1} after 10, 20, 30, 60 and 120 min of acetaldehyde treatment. Different bands appear already after 10 min of dosing, which increase in intensity over time. In Table 4.2 the bands are assigned to specific vibrational frequencies of acetaldehyde and crotonaldehyde.

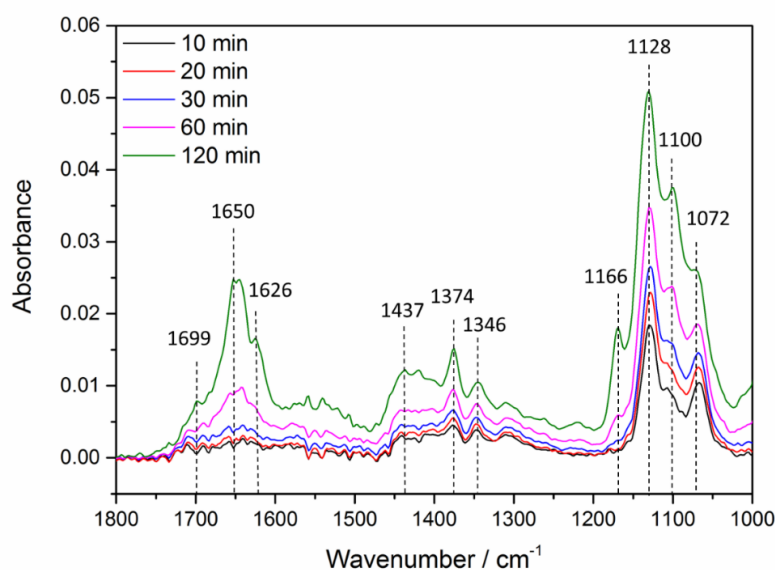


Figure 4.6: ATR-FTIR spectra of an UV-100 film during acetaldehyde treatment in the presence of O_2 and under dry conditions in the dark. Reprinted from Ref.¹²

These band assignments are in accordance to the literature, where also an adsorption of acetaldehyde on the TiO_2 surface has been observed.^{38,39,58} Herein, it has been reported that the oxygen lone pair of the carbonyl group ($C=O$) of acetaldehyde interacts with Ti^{IV} sites. The corresponding vibrational position is located at $\nu(C=O)$ 1699 cm^{-1} . Additionally, further bands characteristic for molecular vibrations of acetaldehyde are detected on the TiO_2 surface such as the $\rho(CH_3)$ at 1072 cm^{-1} , the $\nu(C-C)$ at 1128 cm^{-1} , the $\delta(CH_3)$ at 1346 cm^{-1} , and the $\delta(CH)$ at 1374 cm^{-1} .

In addition to acetaldehyde, bands are assigned to vibrational frequencies of crotonaldehyde, which appear at 1100 cm^{-1} ($\rho(CH_3)$), 1166 cm^{-1} ($\nu(C-C)$), 1437 cm^{-1} ($\delta(CH_3)$), 1626 cm^{-1} ($\nu(C=C)$) and at 1650 cm^{-1} ($\nu(C=O)$). The intensity of these bands ($\nu(C-C)$, $\rho(CH_3)$ and $\nu(C=O)$) shows a higher increase during the second hour of treatment compared to the first hour, because for the formation of crotonaldehyde two acetaldehyde molecules need to be adsorbed on the TiO_2 surface until they are able to react *via* an aldol condensation.³⁶ Thus, a certain time is required until a sufficiently high amount of acetaldehyde molecules are adsorbed on the TiO_2 surface. Considering the decreased concentration of 700 ppb of acetaldehyde detected at the reactor outlet, it is proposed here that the evolved crotonaldehyde is desorbed from the TiO_2 surface, because it is replaced by acetaldehyde molecules that again react to crotonaldehyde. For proving this assumption the gas phase was analysed by MS.

4 Results

Table 4.2: Vibrational frequencies and mode assignments of the observed FTIR bands (cm^{-1}) during acetaldehyde treatment of an anatase Hombikat UV-100 film in the dark.

Position / cm^{-1}	Assignment
1072	$\rho(\text{CH}_3)$ Ti-O=CHCH ₃
1100	$\rho(\text{CH}_3)$ Ti-O=CH(CH) ₂ CH ₃
1128	$\nu(\text{C-C})$ Ti-O=CHCH ₃
1166	$\nu(\text{C-C})$ Ti-O=CH(CH) ₂ CH ₃
1346	$\delta(\text{CH}_3)$ Ti-O=CHCH ₃
1374	$\delta(\text{CH})$ Ti-O=CHCH ₃
1437	$\delta(\text{CH}_3)$ Ti-O=CH(CH) ₂ CH ₃
1626	$\nu(\text{C=C})$ Ti-O=CH(CH) ₂ CH ₃
1650	$\nu(\text{C=O})$ Ti-O=CH(CH) ₂ CH ₃
1699	$\nu(\text{C=O})$ Ti-O=CHCH ₃

An anatase film was treated with acetaldehyde for 25 h and the gas at the reactor outlet was constantly analysed by MS. Figure 4.7 illustrates the time evolution of the QMS signal (41 m/z) corresponding to crotonaldehyde. When acetaldehyde is directed over the UV-100 film, the QMS signal of crotonaldehyde increases until a constant value is reached after 20 h of acetaldehyde treatment. Thus, the generated crotonaldehyde is desorbed from the TiO₂ surface into the gas phase. When the acetaldehyde exposure is stopped, the QMS signal of crotonaldehyde rapidly decreases again, because crotonaldehyde is not formed anymore. Correlating the results obtained from the TiO₂ surface with the ones from the gas phase, it is concluded that acetaldehyde molecules are adsorbed on the TiO₂ surface reacting *via* an aldol condensation to crotonaldehyde which is subsequently desorbed from the surface and is replaced by new acetaldehyde molecules that again react to crotonaldehyde. Thus, the concentration of acetaldehyde detected at the reactor outlet is constantly decreased while the crotonaldehyde concentration increases with dosing time.

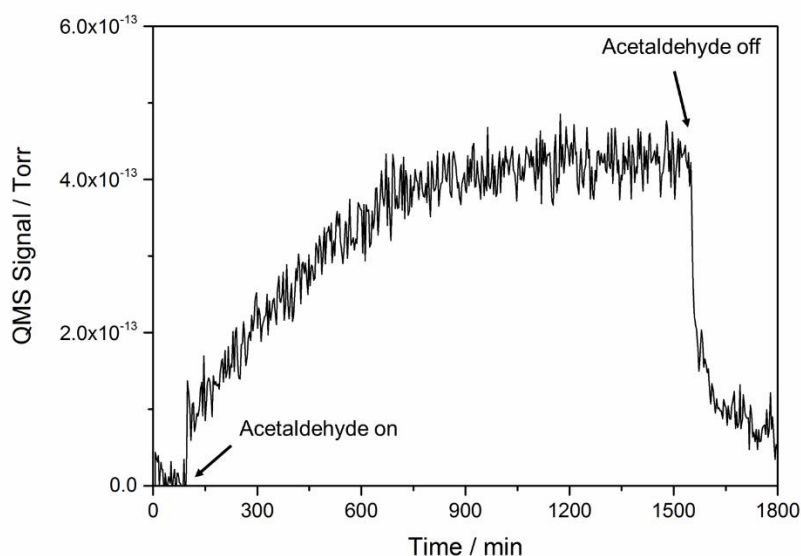


Figure 4.7: Time evolution of the QMS signal corresponding to crotonaldehyde (41 m/z). An UV-100 film is firstly purged with N_2 for 1.5 h, then 50 ppm of acetaldehyde is directed over the UV-100 film for 25 h, before the acetaldehyde exposure is stopped and N_2 is directed again over the film. Reprinted from Ref.¹²

4.3 Adsorption of acetaldehyde and formation of crotonaldehyde on the TiO_2 surface in the presence of water vapor in the dark

In the following section the influence of water vapor on the adsorption of acetaldehyde and the formation of crotonaldehyde on the anatase surface is elucidated. For this purpose, an anatase film was treated with a humidified acetaldehyde gas flow and the acetaldehyde concentration was detected at the reactor outlet. Figure 4.8 illustrates a comparison between the acetaldehyde concentration as a function of the time under dry (left) and humidified conditions (right) in the dark. Under dry conditions the concentration of acetaldehyde is constantly decreased from 1100 ppb to 700 ppb, indicating an adsorption of acetaldehyde on the TiO_2 surface, followed by an aldol condensation forming crotonaldehyde, which is subsequently desorbed from the surface and is replaced by new acetaldehyde molecules. Under humidity a different trend is observed. During the first 15 min of dosing the concentration of acetaldehyde decreases from 1000 ppb to 800 ppb indicating an adsorption of acetaldehyde on the TiO_2 surface. As soon as all adsorption sites are occupied, the concentration of acetaldehyde increases again until the initial value is reached after 1 h. Hence, the adsorption of acetaldehyde is decreased in the presence of water vapor and therefore the formation of crotonaldehyde should also be prevented, because acetaldehyde molecules are not able to react with each other.

4 Results

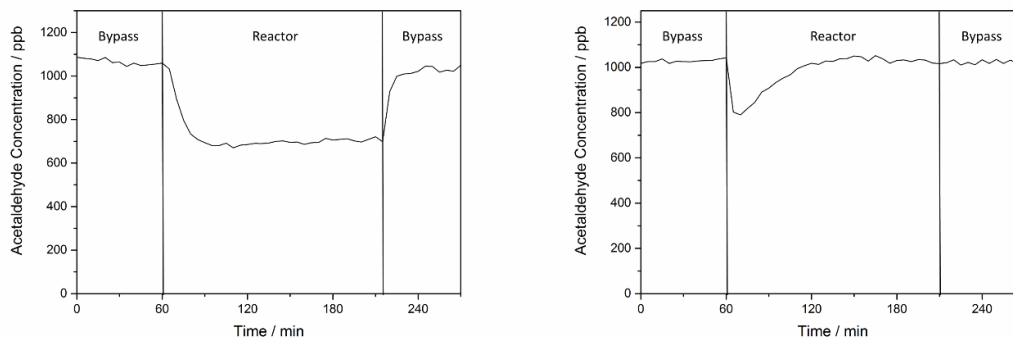


Figure 4.8: Acetaldehyde concentration as a function of the time under dry (left) and humidified (right) conditions in the presence of O_2 in the dark. During the first 60 min the acetaldehyde concentration is kept constant at 1000 ppb in the bypass mode. Afterwards the gas flow is changed to the reactor mode treating an UV-100 film with 1000 ppb of acetaldehyde for 2.5 h, before it is turned back to the bypass mode again. Reprinted from Ref.¹²

A similar experiment was performed in order to gain a deeper understanding of the effect of water vapor on the adsorption of acetaldehyde. Herein, an anatase film was treated with acetaldehyde under dry conditions in the dark and the concentration of acetaldehyde was detected at the reactor outlet. The corresponding time evolution of the acetaldehyde concentration is shown in Figure 4.9. At the beginning the concentration was kept constant at 1 ppm in the bypass mode for 1 h. Afterwards the gas mixture was directed over the anatase sample for 12 h allowing the acetaldehyde molecules to adsorb and to react to crotonaldehyde. The gas flow was then changed to the bypass mode and a washing bottle was inserted into the system, in order to generate a humidified acetaldehyde gas flow. When the gas mixture was directed again over the TiO_2 film, the concentration of acetaldehyde strongly increased from 1 ppm to 6.3 ppm and subsequently decreased to the value of 1 ppm again. Thus, in the presence of water vapor, acetaldehyde molecules are desorbed from the TiO_2 surface, because water is favorably adsorbed. A decreased concentration of acetaldehyde is not detected at the reactor exit, since acetaldehyde molecules do not react to crotonaldehyde anymore. Moreover, since a huge amount of water is present on the TiO_2 surface, the equilibrium of the aldol condensation shifts to the educt site, leading also to a decrease in the formation of crotonaldehyde.

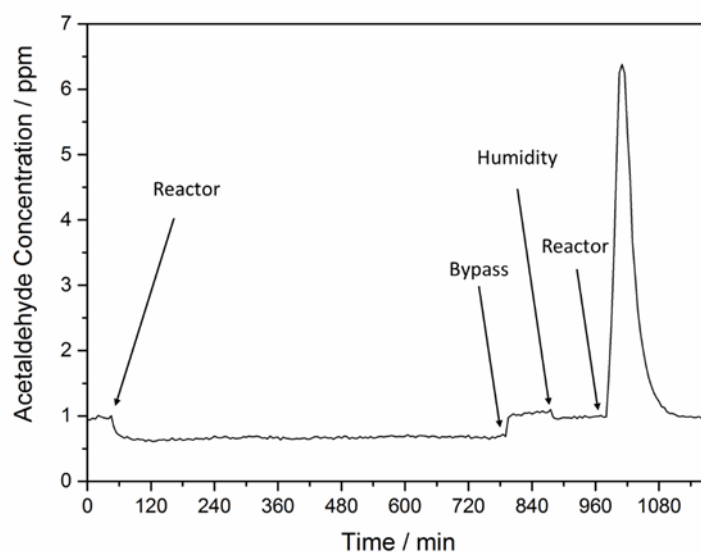


Figure 4.9: Concentration of acetaldehyde as a function of the time in the presence of O_2 in the dark. During the first 60 min the concentration of acetaldehyde is kept constant at 1 ppm in the bypass mode. Afterwards the gas is directed over the anatase film for 12 h, before turning back to the bypass mode again. A washing bottle is inserted into the system, generating a humidified acetaldehyde gas flow, which is then directed over the TiO_2 film again using the reactor mode. Reprinted from Ref.¹²

For a further verification of the preferential adsorption of water compared to acetaldehyde on the TiO_2 surface, the latter experiment was repeated and ATR-FTIR spectra of a TiO_2 film were recorded. Figure 4.10 illustrates a spectrum of an anatase film (black) after an acetaldehyde treatment for 2 h under dry conditions in the dark. As expected bands characteristic for acetaldehyde and crotonaldehyde are observed. A washing flask was then inserted into the system, in order to generate a humidified acetaldehyde gas flow, which was directed over the TiO_2 film. The intensity of the bands characteristic for acetaldehyde and crotonaldehyde decrease immediately within 5 min of treatment, indicating a fast desorption of acetaldehyde and crotonaldehyde from the anatase surface because water is favorably adsorbed. Thus, the ATR-FTIR results confirm the GC analysis.

The following experiments are performed under dry conditions, because water vapor decreases the adsorption of acetaldehyde and prevents the formation of crotonaldehyde on the TiO_2 surface.

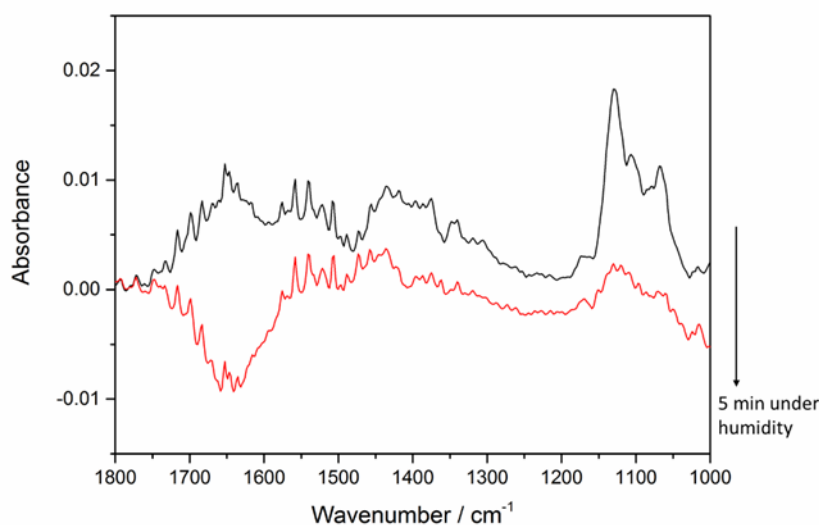


Figure 4.10: ATR-FTIR spectrum of an anatase film recorded after acetaldehyde treatment for 2 h under dry conditions and in the presence of O_2 in the dark (black). Afterwards a humidified acetaldehyde gas flow was directed over the TiO_2 film and a spectrum was recorded after 5 min of treatment (red). Reprinted from Ref.¹²

4.4 Adsorption of acetaldehyde and formation of crotonaldehyde on the anatase surface in the presence and absence of O_2 in the dark

In addition to the effect of water vapor, in the following the influence of molecular O_2 on the adsorption of acetaldehyde and the formation of crotonaldehyde over TiO_2 is examined. For this purpose an anatase film was treated with acetaldehyde in O_2 and in N_2 atmosphere for 2.5 h in the dark and the concentration of acetaldehyde was detected at the reactor outlet. Figure 4.11 shows the time evolution of the acetaldehyde concentration in O_2 (left) and N_2 (right) atmosphere. Both curves show a similar trend. At the beginning the concentration of acetaldehyde is kept constant at 1100 ppb using the bypass mode. After 1 h the gas is directed over the anatase sample leading to a decrease in the concentration from 1100 ppb to 700 ppb, thus, both, in O_2 and N_2 atmosphere, acetaldehyde is adsorbed on the TiO_2 surface reacting *via* an aldol condensation to crotonaldehyde, which is desorbed from the surface and is replaced by new acetaldehyde molecules that again react with each other. When the gas flow is turned back to the bypass mode, the concentration of acetaldehyde increases to its initial value of 1100 ppb.

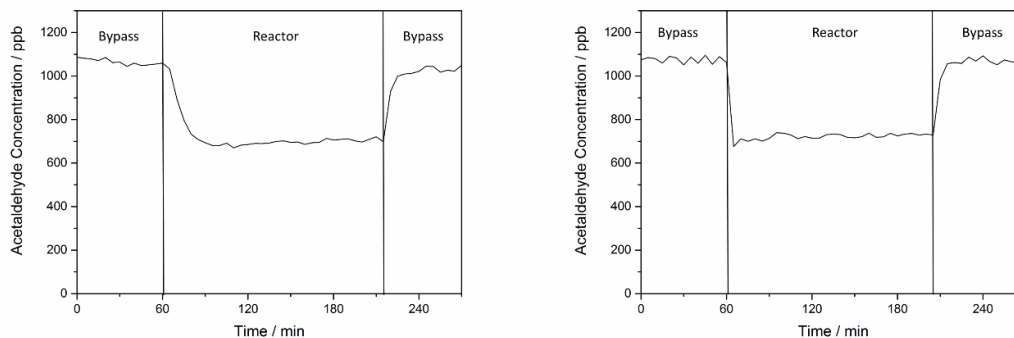


Figure 4.11: Time evolution of the acetaldehyde concentration in O₂ (left) and N₂ (right) atmosphere after directing the gas over an anatase film in the dark. During the first 60 min the acetaldehyde concentration is kept constant at 1100 ppb in the bypass mode. Afterwards the gas is directed over an UV-100 film for 2.5 h using the reactor mode, before it is turned back to the bypass mode again. Reprinted from Ref.¹²

Besides the gas analysis, ATR-FTIR spectra of an UV-100 film were recorded during acetaldehyde treatment in O₂ and in N₂ atmosphere for 2 h in the dark (see Figure 4.12). Both spectra show bands characteristic for molecular vibrations of acetaldehyde and crotonaldehyde with similar intensities. Hence, according to the gas and surface analyses, the presence of molecular O₂ does not have an effect on the adsorption of acetaldehyde and the formation of crotonaldehyde on the TiO₂ surface.

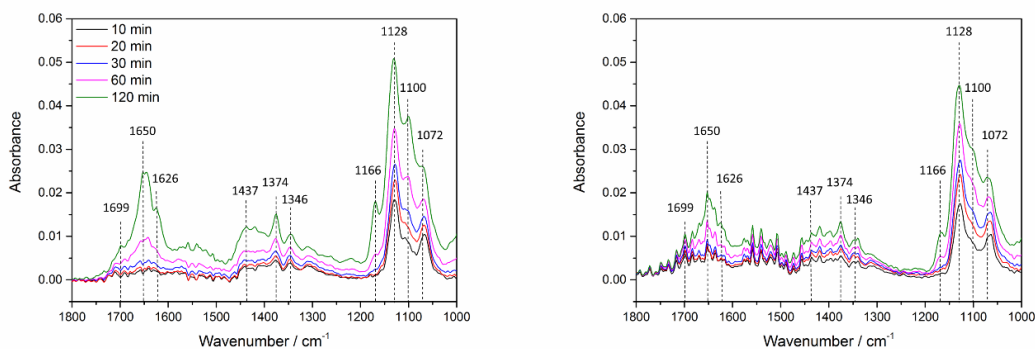


Figure 4.12: ATR-FTIR spectra of an UV-100 recorded during acetaldehyde treatment in O₂ (left) and N₂ (right) atmosphere for 2 h in the dark. Reprinted from Ref.¹²

4.5 Photocatalytic degradation of acetaldehyde in the presence and absence of molecular O₂

After the processes in the dark have been investigated, in the following the effect of molecular O₂ on the degradation of acetaldehyde over TiO₂ is investigated upon UV illumination. For this purpose, an anatase film was treated with acetaldehyde in O₂ and in N₂ atmosphere for 6 h upon UV illumination and the concentration of acetaldehyde was

4 Results

detected at the reactor outlet. Figure 4.13 illustrates the time evolution of the acetaldehyde concentration in O₂ (left) and in N₂ (right) atmosphere. At the beginning of the illumination time the acetaldehyde concentration decreases from 700 ppb to 580 ppb in both atmospheres, indicating a degradation of acetaldehyde over TiO₂. In the presence of O₂ this value remains constant during illumination time, because acetaldehyde is constantly degraded. In contrast, in N₂ atmosphere the concentration of acetaldehyde increases after 30 min upon UV illumination reaching a value of 620 ppb at the end of illumination time, because acetaldehyde is incompletely degraded in the absence of O₂. When the UV light is turned off again the initial value is reached again and acetaldehyde is not degraded anymore.

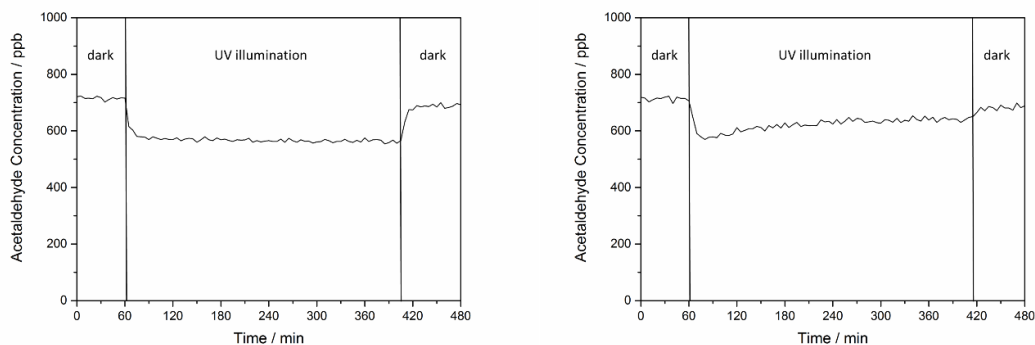


Figure 4.13: Concentration of acetaldehyde as a function of the time in O₂ (left) and N₂ (right) atmosphere in the dark and upon UV illumination. Reprinted from Ref.¹²

For a better understanding of the degradation mechanism of acetaldehyde on the TiO₂ surface, ATR-FTIR spectra of an UV-100 film treated with acetaldehyde in O₂ and in N₂ atmosphere were recorded upon 6 h of UV illumination. The corresponding ATR-FTIR spectra in O₂ (left) and in N₂ (right) atmosphere are illustrated in Figure 4.14. In Table 4.3 the positions of the bands are assigned to specific molecular vibrations of intermediates formed during the decomposition of acetaldehyde. Upon UV illumination the bands characteristic for acetaldehyde decrease in intensity because acetaldehyde is degraded over TiO₂. Simultaneously, new bands appear which increase in intensity with illumination time. These bands are assigned to molecular vibrations of acetate and formate. Herein, the $\nu_s(\text{COO})$ and the $\nu_{as}(\text{COO})$ of acetate as well as the $\nu(\text{C=O})$ of acetic acid show a similar trend in intensity in O₂ and in N₂ atmosphere. In contrast, the $\nu_s(\text{COO})$ and the $\nu_{as}(\text{COO})$ of formate appear similar in intensity during the first 30 min in both atmospheres (black to purple), but afterwards the bands show a higher increase in O₂

atmosphere than in N_2 atmosphere. Thus, in the absence of molecular O_2 acetate and formate are generated during the first 30 min upon UV illumination, but afterwards the formation of formate decreases, because acetate is not converted into formate anymore.

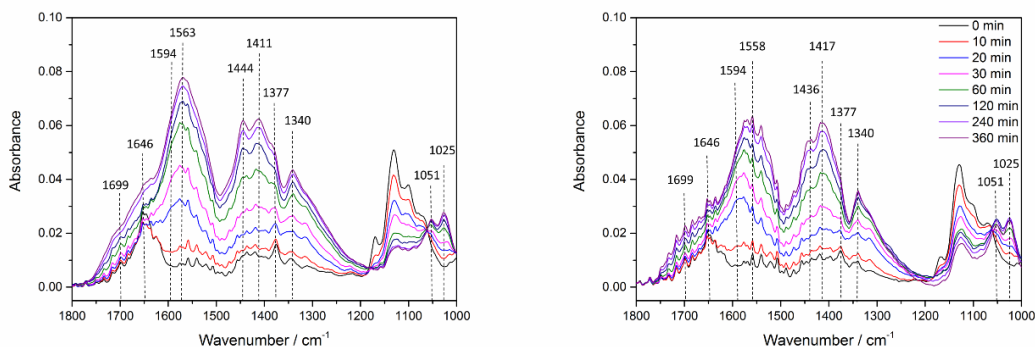


Figure 4.14: ATR-FTIR spectra of an UV-100 film recorded during acetaldehyde treatment in O_2 (left) and N_2 (right) atmosphere upon 6 h of UV illumination. Reprinted from Ref.¹²

When correlating surface and gas analysis, it is proposed that under oxygenic conditions acetaldehyde is constantly degraded into acetate/acetic acid and formate, because a sufficiently high amount of O_2 is available on the TiO_2 surface for oxidation reactions. In N_2 atmosphere surface adsorbed O_2 is consumed for the formation of acetate and formate during the first 30 min upon UV illumination. As soon as all adsorbed O_2 molecules have reacted, O_2 is depleted on the TiO_2 surface and acetate is not converted into formate anymore. It is rather accumulated on the TiO_2 surface, thus acetaldehyde is incompletely degraded and the concentration at the reactor outlet increases. It is proposed here that a bridging oxygen atom from the TiO_2 surface is consumed for the formation of acetate in the absence of molecular O_2 .

4 Results

Table 4.3: Vibrational frequencies and mode assignments of the observed FTIR bands (cm^{-1}) of an anatase Hombikat UV-100 film during acetaldehyde treatment and UV illumination.

Position / cm^{-1}	Assignment
1025	$\rho(\text{CH}_3) \text{CH}_3\text{COO}^-$
1051	$\nu(\text{C-C}) \text{CH}_3\text{COO}^-$
1340	$\nu_s(\text{COO}) \text{HCOO}^-$
1377	$\nu(\text{C-H}) \text{HCOO}^-$
1411/1417	$\delta(\text{CH}_3) \text{CH}_3\text{COO}^-$
1436/1444	$\nu_s(\text{COO}) \text{CH}_3\text{COO}^-$
1558/1563	$\nu_{as}(\text{COO}) \text{CH}_3\text{COO}^-$
1594	$\nu_{as}(\text{COO}) \text{HCOO}^-$
1646	$\delta(\text{H}_2\text{O})$
1699	$\nu(\text{C=O}) \text{CH}_3\text{COOH}$

4.6 Photodesorption of crotonaldehyde from the TiO_2 surface

The ATR-FTIR spectra in Figure 4.14 also show, that besides acetaldehyde the bands characteristic for crotonaldehyde decrease in intensity upon UV illumination suggesting a decomposition of crotonaldehyde over TiO_2 . However, this assumption is not confirmed by MS. Herein, an UV-100 film was treated with acetaldehyde in N_2 atmosphere for 2 h in the dark allowing the acetaldehyde molecules to adsorb and to react to crotonaldehyde on the TiO_2 surface. Afterwards the sample is illuminated by UV light for 3 h, followed by a dark period of 1 h again. Figure 4.15 shows the time evolution of the QMS signal corresponding to crotonaldehyde (41 m/z) detected at the reactor outlet. Upon UV illumination the QMS signal rapidly increases within the first 10 min and then decreases again indicating that upon UV illumination crotonaldehyde is desorbed from the TiO_2 surface into the gas phase.

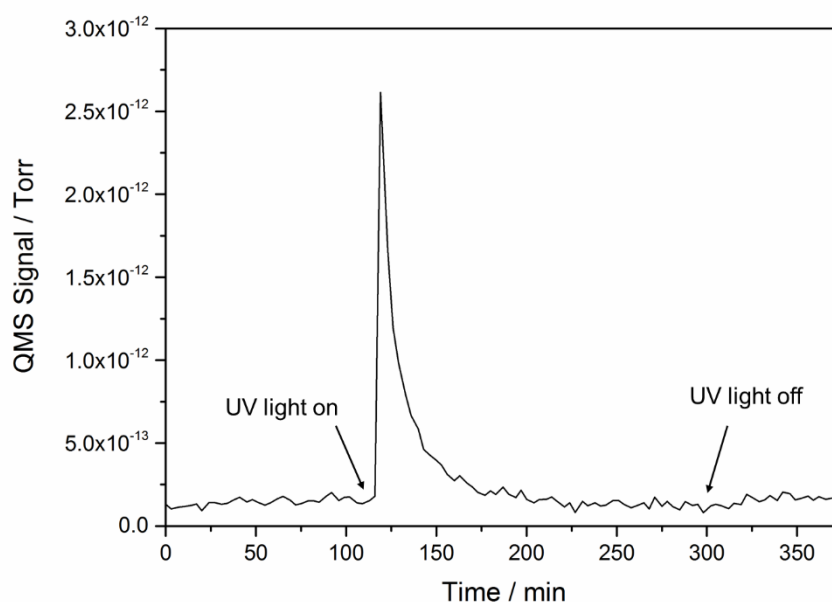


Figure 4.15: QMS signal of crotonaldehyde (41 m/z) as a function of the time in the dark and upon UV illumination. The gas at the reactor outlet was constantly analysed by MS during acetaldehyde treatment of an UV-100 film in the absence of O₂.

4.7 Evolution of gaseous products during the photocatalytic degradation of acetaldehyde over TiO₂ in the absence of molecular O₂

In addition to crotonaldehyde, further gases were detected at the reactor outlet during acetaldehyde degradation over TiO₂ in the absence of molecular O₂. Figure 4.16 illustrates the time evolution of the QMS signal corresponding to CH₄ (16 m/z). Upon UV illumination the QMS signal strongly increases within the first 30 min and afterwards decreases again until a stable value is reached at the end of illumination time. The fast evolution at the beginning of the illumination may result from the degradation of acetaldehyde molecules adsorbed during the dark period. As soon as the adsorbed acetaldehyde molecules have reacted, the QMS signal decreases because new acetaldehyde molecules need to reach the TiO₂ surface. At the end of illumination time a constant value is observed evincing that equilibrium has been reached. When turning off the UV light again, the QMS signal further decreases to its initial value. Hence, MS

4 Results

analysis reveals the formation of CH_4 during the photocatalytic degradation of acetaldehyde over TiO_2 in the absence of molecular O_2 .

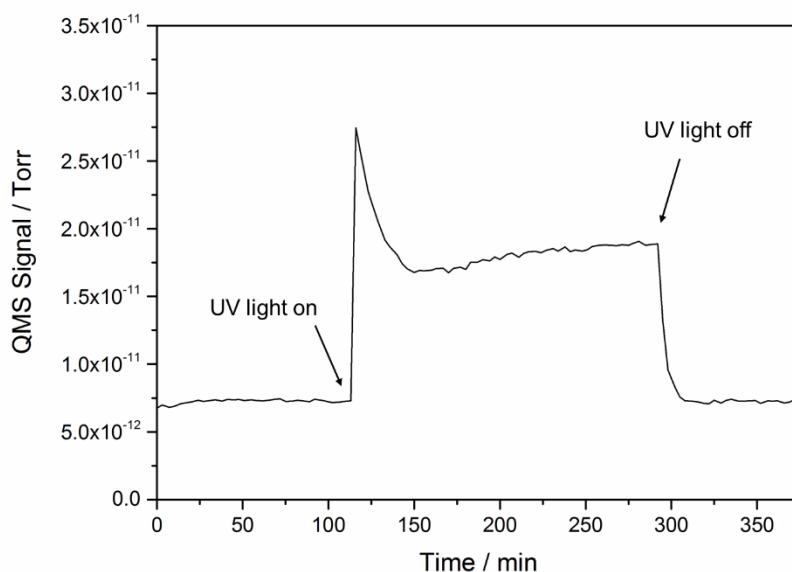


Figure 4.16: Time evolution of the QMS signal of CH_4 (16 m/z) evolved during the photocatalytic degradation of acetaldehyde over TiO_2 in the absence of O_2 . Reprinted from Ref.¹²

Besides the evolution of CH_4 , CO_2 is also detected at the reactor outlet. Figure 4.17 illustrates the QMS signals of C^{16}O_2 (44 m/z) and the isotopologues $\text{C}^{18}\text{O}^{16}\text{O}$ (46 m/z) as a function of the time. During the first 30 min upon UV illumination of the UV-100 film a fast evolution of CO_2 occurs resulting from the reaction of acetaldehyde molecules with surface-adsorbed O_2 . As soon as all adsorbed O_2 molecules have reacted, O_2 is depleted on the surface and thus the formation of CO_2 rapidly decreases. When the UV-light is turned off, the QMS signal further decreases to its initial value. Accordingly, upon UV illumination acetaldehyde is photocatalytically decomposed into CO_2 in the absence of molecular O_2 .

When correlating the surface and the gas phase analysis, it is concluded that in the absence of molecular O_2 acetaldehyde reacts with surface adsorbed O_2 to acetate, formate, and eventually CO_2 during the first 30 min upon UV illumination. When all the adsorbed O_2 molecules have been consumed, O_2 is depleted on the TiO_2 surface and acetate is not converted into formate anymore. It is rather accumulated on the TiO_2 surface, where it partly decomposes into CH_4 and CO_2 .

Acetate is most likely formed by a reaction of adsorbed acetaldehyde with a lattice oxygen atom from the TiO_2 surface. Thus, CO_2 should contain a bridging oxygen atom from the TiO_2 lattice. For proving this assumption isotopic studies using Ti^{18}O_2 have been performed.

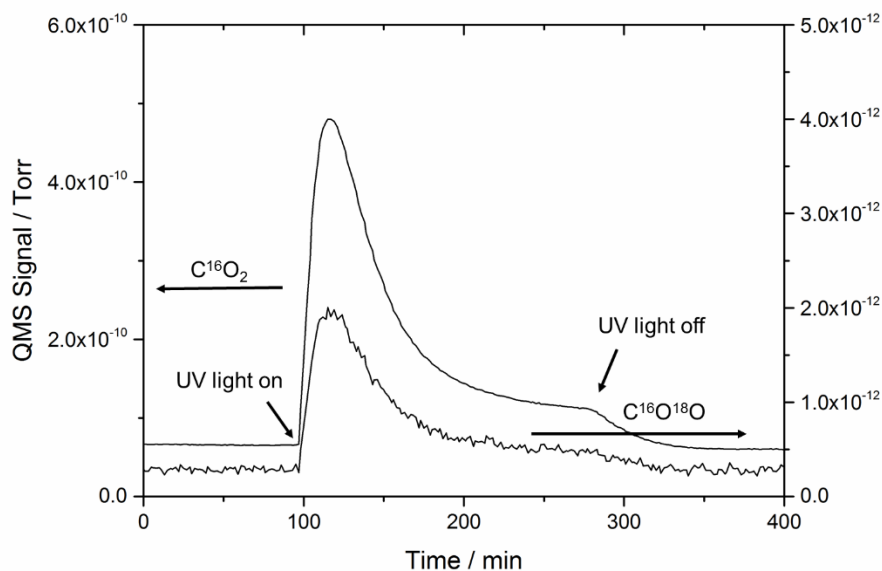


Figure 4.17: Time evolution of the QMS signal of C^{16}O_2 (44 m/z) and the isotopologues $\text{C}^{18}\text{O}^{16}\text{O}$ (46 m/z) during photocatalytic degradation of acetaldehyde over UV-100 (Ti^{16}O_2) in the absence of O_2 . Reprinted from Ref.⁵⁷

A schematic illustration of the hydroxylated surface of Ti^{18}O_2 is shown in Figure 4.18. Two types of oxygen species exist on the TiO_2 surface: the terminal oxygen atoms and the bridging oxygen atoms. The terminal oxygen atom can be removed by heating up to 623 K while the bridging oxygen atoms remain stable up to 773 K. The synthesized Ti^{18}O_2 contains terminal oxygen atoms $^{16}\text{O}_t^-$ and bridging oxygen atoms $^{18}\text{O}_{\text{br}}^{2-}$, because Ti^{18}O_2 was calcined at 623 K, therefore, the terminal oxygen atoms were mostly removed from the surface while the bridging oxygen atoms remain stable at this temperature. Further washing with H_2^{16}O induces a replacement of the remaining $^{18}\text{O}_t^-$ atoms by $^{16}\text{O}_t^-$ atoms from water.³⁰

4 Results

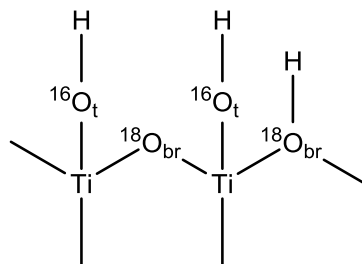


Figure 4.18: Schematic illustration of the hydroxylated surface of Ti^{18}O_2 . Reprinted from Ref. ⁵⁷

Ti^{18}O_2 and UV-100 (Ti^{16}O_2) were treated with acetaldehyde for 2 h in the dark, followed by UV illumination for 3 h, before turning back to the dark mode again. During this process the evolved C^{16}O_2 (44 m/z) and $\text{C}^{18}\text{O}^{16}\text{O}$ (46 m/z) were monitored at the reactor outlet by MS. Figure 4.17 and Figure 4.19 show the time evolution of the QMS signals of C^{16}O_2 (44 m/z) and $\text{C}^{18}\text{O}^{16}\text{O}$ (46 m/z) corresponding to Ti^{16}O_2 (UV-100) and Ti^{18}O_2 , respectively. When comparing the trends of the C^{16}O_2 and $\text{C}^{18}\text{O}^{16}\text{O}$ curves, they appear similar except that the $\text{C}^{18}\text{O}^{16}\text{O}$ signal is two orders of magnitude lower than the C^{16}O_2 signal, because of the natural abundance of $\text{C}^{18}\text{O}^{16}\text{O}$ in C^{16}O_2 . Both, UV-100 and the isotopologues Ti^{18}O_2 exhibit a fast CO_2 evolution at the beginning of the UV illumination, because acetaldehyde molecules react with surface-adsorbed O_2 forming acetate, formate, and eventually CO_2 . As soon as O_2 is depleted on the TiO_2 surface, the CO_2 evolution decreases. When the UV light is turned off, the QMS signals reach the initial values again. In order to figure out, whether bridging oxygen atoms are incorporated into CO_2 , the QMS signal ratio was calculated according to the following equation:

$$\text{QMS signal ratio} / \% : \frac{\frac{m}{z} = 46(\text{C}^{18}\text{O}^{16}\text{O})}{\frac{m}{z} = 44(\text{C}^{16}\text{O}_2)} \times 100 \quad (15)$$

The corresponding QMS signal ratios of Ti^{16}O_2 and Ti^{18}O_2 as a function of the time are illustrated in Figure 4.20. In the dark both samples exhibit a similar ratio of 0.45 % due to the natural abundance of $\text{C}^{18}\text{O}^{16}\text{O}$ in C^{16}O_2 . Upon UV illumination the ratio of the Ti^{18}O_2 increases from 0.45 % to 0.56 % during the first 30 min, remains then constant for 1 h before it decreases again to 0.51% at the end of illumination time. When turning off the UV light, the ratio further decreases to its initial value of 0.45 %. In contrast, Ti^{16}O_2 exhibits a constant ratio of 0.45 % in the dark and upon illumination. The increased ratio of Ti^{18}O_2 upon UV illumination clearly proves an incorporation of bridging oxygen $^{18}\text{O}_{\text{br}}^{2-}$ atoms into CO_2 , because Ti^{18}O_2 is the only $^{18}\text{O}_{\text{br}}^{2-}$ source. It is proposed that upon UV

illumination holes are trapped as $O_{br}^{\bullet-}$, which react with adsorbed acetaldehyde forming acetate that is further decomposed into CO_2 . The remaining oxygen vacancy is replenished by an oxygen atom supplied from adsorbed $H_2^{16}O$, because during UV illumination the $C^{18}O^{16}O/C^{16}O_2$ ratio of the $Ti^{18}O_2$ decreases. The replenished bridging oxygen atom $^{16}O_{br}^{2-}$ acts as new trapping site for a hole forming $^{16}O_{br}^{\bullet-}$ which further reacts with acetaldehyde to acetate and eventually $C^{16}O_2$. Accordingly, the $C^{18}O^{16}O/C^{16}O_2$ ratio decreases with illumination time, because only a limited amount of $^{18}O_{br}^{2-}$ atoms is available for the reaction with acetaldehyde.

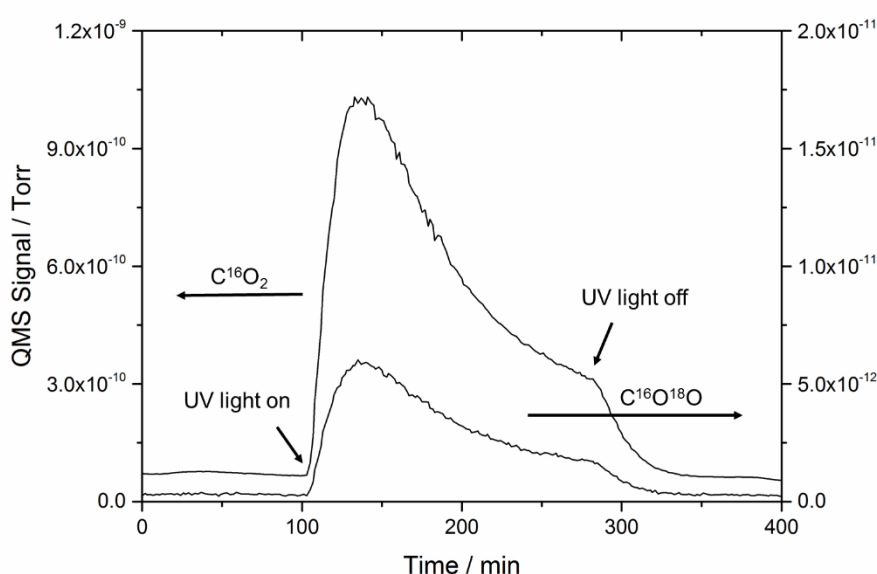


Figure 4.19: Time evolution of the QMS signal from $C^{16}O_2$ (44 m/z) and the isotopologues $C^{18}O^{16}O$ (46 m/z) during photocatalytic degradation of acetaldehyde over $Ti^{18}O_2$ in the absence of O_2 . Reprinted from Ref.⁵⁷

The number of $^{18}O_{br}^{2-}$ atoms incorporated into the evolved CO_2 is calculated for $Ti^{18}O_2$. For this purpose the QMS signal of the $C^{16}O_2$ curve of $Ti^{18}O_2$ is converted into a rate ($\mu\text{mol/h}$) of CO_2 production by performing a calibration with a standard $C^{16}O_2$ gas (see Figure 4.21). Figure 4.22 shows the calculated CO_2 rate as a function of the time. The total amount of $C^{16}O_2$ produced during the photocatalytic degradation of acetaldehyde is determined by an integration in the time range between 1.7 h and 5 h yielding a value of $4.29 \mu\text{mol } C^{16}O_2$. A further integral in the same time range is performed for the $C^{18}O^{16}O/C^{16}O_2$ ratio of $Ti^{18}O_2$ (see Figure 4.20) obtaining a value of 0.32 %. The total amount of $C^{18}O^{16}O$ photogenerated is calculated according to equation 16:

4 Results

$$C^{18}O^{16}O (\mu\text{mol}) = C^{16}O_2 (\mu\text{mol}) \times \frac{{}^{18}O(\%)}{100} \quad (16)$$

0.014 μmol $C^{18}O^{16}O$ are evolved during the photodegradation of acetaldehyde on the $Ti^{18}O_2$ surface. Since $Ti^{18}O_2$ is the only ^{18}O source, the amount of exchanged oxygen atoms can be calculated according to the following equation:

$${}^{18}O_{\text{br}} \text{ atoms exchanged} = C^{18}O^{16}O (\mu\text{mol}) \times \frac{6.022 \times 10^{17} \text{ atoms}}{1 \mu\text{mol}} \quad (17)$$

8.16×10^{15} bridging oxygen atoms from the TiO_2 lattice are incorporated into CO_2 . Montoya *et al.*¹⁵ observed a similar value of 9.33×10^{15} oxygen atoms which were exchanged during the photocatalytic degradation of benzene under anaerobic conditions.

Hence, this work strongly supports the incorporation of bridging oxygen atoms from the TiO_2 lattice into CO_2 during the photocatalytic degradation of gaseous acetaldehyde. Upon UV illumination adsorbed acetaldehyde molecules react with bridging oxygen atoms forming acetate and eventually CO_2 .

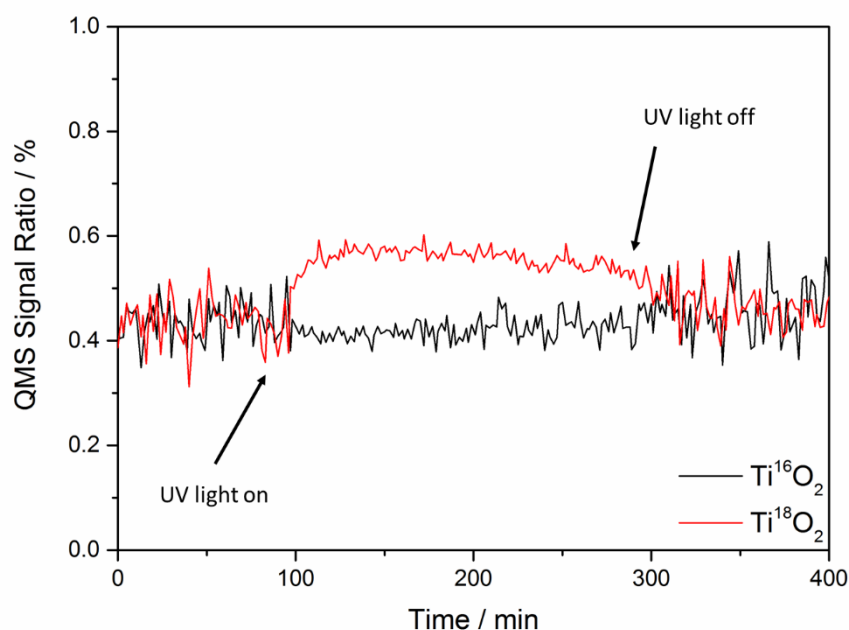


Figure 4.20: QMS signal ratio of $Ti^{16}O_2$ and $Ti^{18}O_2$ during the photocatalytic degradation of acetaldehyde in the absence of molecular O_2 . Adapted from Ref.⁵⁷

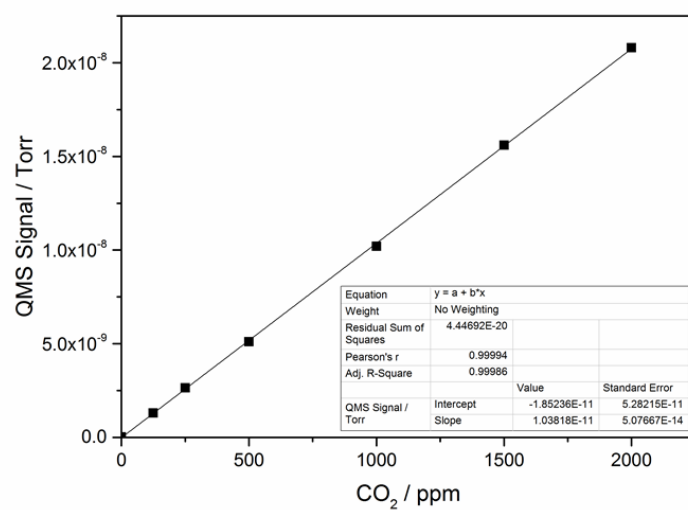


Figure 4.21: Calibration curve of $C^{16}O_2$.

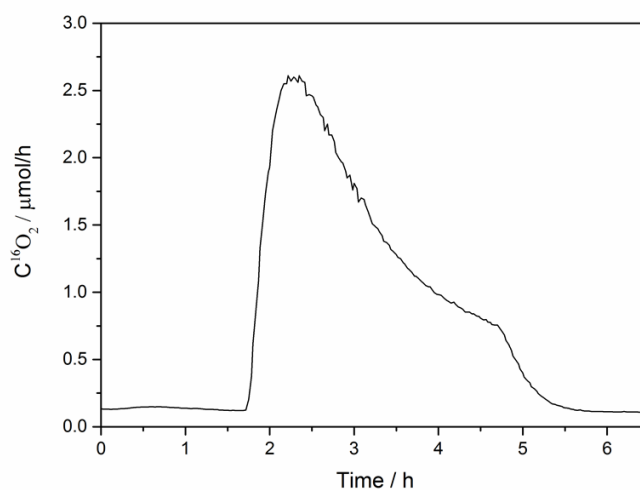


Figure 4.22: Production rate of $C^{16}O_2$ ($\mu\text{mol/h}$) during the photocatalytic degradation of acetaldehyde over $Ti^{18}O_2$ in the absence of O_2 . Reprinted from Ref.⁵⁷

4 Results

5 Discussion

This chapter begins with a discussion of the adsorption of acetaldehyde and the formation of crotonaldehyde on the TiO₂ surface in the dark. In particular, it is elucidated how water vapor and molecular O₂ affect the surface processes in the dark. In the second part, the degradation mechanism of acetaldehyde in the presence and absence of O₂ is discussed in order to understand the role of molecular O₂ in the photocatalytic degradation process of acetaldehyde. In this context, it is clarified whether lattice oxygen atoms from the TiO₂ surface are involved in the photocatalytic degradation process of acetaldehyde.

5.1 Acetaldehyde adsorption and crotonaldehyde formation under dry conditions in the dark

When an UV-100 film is treated with acetaldehyde in O₂ atmosphere under dry conditions in the dark, the acetaldehyde concentration detected at the reactor outlet is constantly decreased from 1100 ppb to 700 ppb (see Figure 4.4). Interestingly, the concentration does not increase to the initial value again even after several hours of acetaldehyde gas treatment (see Figure 4.5). ATR-FTIR spectra were recorded of an UV-100 film treated with acetaldehyde for 2 h under dry conditions in the dark, in order to figure out the reason for the constantly decreased concentration of acetaldehyde. The spectra (shown in Figure 4.6) reveal an adsorption of acetaldehyde on the anatase surface. Acetaldehyde adsorption on the TiO₂ surface occurs in two different ways: either the carbonyl group of acetaldehyde interacts molecularly *via* hydrogen bonds with surface hydroxyl groups from TiO₂ or acetaldehyde is adsorbed in a more stable way through its oxygen lone pair on Ti^{IV} sites (see chapter 2.3).^{32,36} The shift of the $\nu(\text{C}=\text{O})$ of acetaldehyde from 1761 cm⁻¹ in the gas phase³⁹ to lower wavenumbers of 1699 cm⁻¹ (see Table 4.2) clearly proves the interaction between the oxygen lone pair of the carbonyl group of acetaldehyde and Ti^{IV} sites of TiO₂.³⁶ Besides $\nu(\text{C}=\text{O})$ further bands characteristic for acetaldehyde such as $\rho(\text{CH}_3)$, $\nu(\text{C}-\text{C})$, $\delta(\text{CH}_3)$, and $\delta(\text{CH})$ are observed, which increase in intensity with dosing time revealing also an adsorption of acetaldehyde on the TiO₂ surface.

In addition to acetaldehyde, ATR-FTIR spectra show bands characteristic for the molecular vibrations of crotonaldehyde (see Table 4.2). These findings are in accordance to the literature, where crotonaldehyde has also been observed on the TiO₂ surface by FTIR spectroscopy.^{36,38,39,59} Idriss *et al.*⁷ proposed that two acetaldehyde molecules adsorbed on the TiO₂ surface react *via* an aldol condensation to crotonaldehyde. This reaction is initiated by a bridging oxygen atom from the TiO₂, which acts as a base

5 Discussion

abstracting one proton from the carbonyl group of an adsorbed acetaldehyde molecule (see chapter 2.3). The thus generated crotonaldehyde molecule is adsorbed through its oxygen lone pair on Ti^{IV} sites as is evidenced by a shift in the $\nu(\text{C}=\text{O})$ of crotonaldehyde from 1725 cm^{-1} in the gas phase to lower wavenumbers of 1650 cm^{-1} .⁶⁰ Thus, acetaldehyde and crotonaldehyde are both adsorbed at the same adsorption sites on the TiO_2 surface.

Besides the processes occurring on the TiO_2 surface the gas at the reactor outlet was also analysed by MS. Figure 4.7 shows the QMS signal corresponding to crotonaldehyde. The signal steadily increases during acetaldehyde treatment and rapidly decreases, when acetaldehyde dosing is stopped. Thus, the formed crotonaldehyde is obviously desorbed from the TiO_2 surface, because it is detected in the gas phase by MS.

The results obtained from the TiO_2 surface are correlated with the gas phase analyses and a reaction mechanism is proposed which is illustrated in Figure 5.1. Herein, it is suggested that acetaldehyde molecules are firstly adsorbed on the TiO_2 surface under dry conditions in the dark. When two neighboring acetaldehyde molecules are adsorbed, they are able to react *via* an aldol condensation forming crotonaldehyde (see section 2.3). Acetaldehyde and crotonaldehyde both are adsorbed through their oxygen lone pairs on Ti^{IV} sites resulting in a competition for adsorption sites. Hence, the continuous acetaldehyde gas flow leads to a replacement of the generated crotonaldehyde molecules by acetaldehyde molecules, which has been evidenced by an increase in the concentration of crotonaldehyde in the gas phase by MS. The newly adsorbed acetaldehyde molecules react again to crotonaldehyde leading to a constantly low concentration of acetaldehyde at the reactor outlet detected by GC/PID.

Rekoske *et al.*⁵⁹ investigated the competition between acetaldehyde and crotonaldehyde on anatase and rutile TiO_2 surfaces by FTIR spectroscopy. These authors observed the formation of crotonaldehyde on the rutile surface at 313 K, but did not observe this process on the anatase surface, apparently because higher temperatures of 373 K are required here. In the present study the formation of crotonaldehyde on the anatase surface was observed at RT. Rekoske *et al.* showed that both, crotonaldehyde and acetaldehyde adsorb in a similar fashion and that they can be readily displaced by the respective other aldehyde from the TiO_2 surface, which is in accordance to the results obtained in this study.

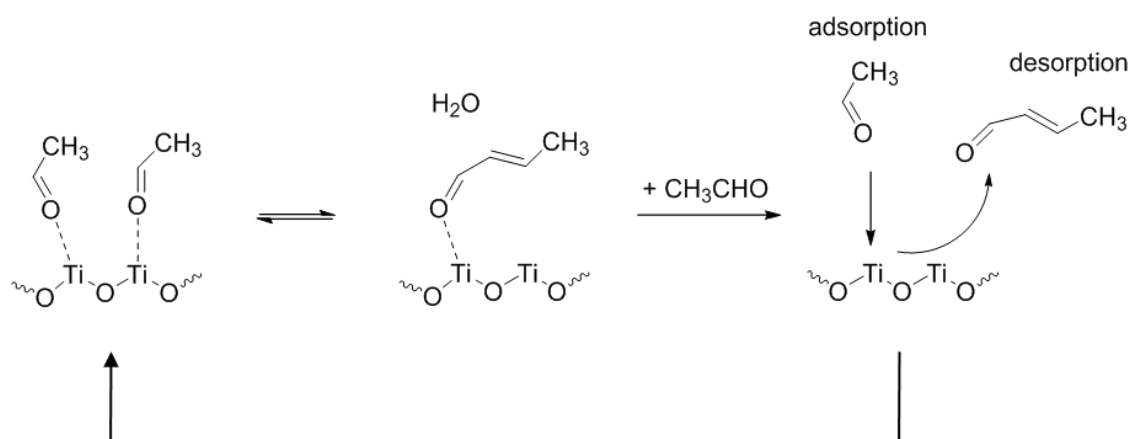


Figure 5.1: Schematic illustration of the surface processes occurring under dry conditions in the dark when an UV-100 film is treated with acetaldehyde in O_2 atmosphere. After the adsorption of acetaldehyde molecules on the TiO_2 surface, they react *via* an aldol condensation forming crotonaldehyde, which is desorbed from the surface and is replaced by new acetaldehyde molecules that again react to crotonaldehyde. Reprinted from Ref.¹²

5.2 Effect of water vapor on the adsorption of acetaldehyde and the formation of crotonaldehyde

After the mode of adsorption as well as the surface catalyzed aldol condensation of acetaldehyde have been clarified under dry conditions in the dark, in the following section the effect of water vapor on the adsorption of acetaldehyde and on the formation of crotonaldehyde is elucidated. For this purpose an UV-100 film was treated with 1000 ppb of acetaldehyde in the presence of water vapor and the concentration of acetaldehyde was detected at the reactor outlet by GC/PID. Figure 4.8 shows on the right that the concentration of acetaldehyde firstly decreases from 1000 ppb to 800 ppb and then increases to its initial value. Thus, acetaldehyde molecules are adsorbed on the TiO_2 surface until all adsorption sites are occupied leading to an increase of the acetaldehyde concentration at the reactor outlet. Sofianou *et al.*⁶¹ and Horikoshi *et al.*⁶² also observed a brief decrease in the acetaldehyde concentration when TiO_2 was exposed to a humidified acetaldehyde gas flow of 1000 ppb, which they explained by an adsorption of acetaldehyde molecules on the TiO_2 surface. When comparing the time evolution curves of acetaldehyde under dry and humid conditions, it can be seen that the adsorption of acetaldehyde on the TiO_2 surface is much lower in the presence of water vapor as in its absence.

For a better understanding of the effect of water vapor on the adsorption of acetaldehyde and on the formation of crotonaldehyde on the TiO_2 surface, the experiment shown in

5 Discussion

Figure 4.4 was repeated and an anatase film was treated with 1000 ppb of acetaldehyde under dry conditions in the dark. Figure 4.9 shows that the acetaldehyde concentration detected at the reactor outlet is constantly decreased to 700 ppb evincing an adsorption of acetaldehyde and the formation of crotonaldehyde on the TiO_2 surface. Thus, both acetaldehyde and crotonaldehyde are present on the TiO_2 surface. The gas flow was then changed from the reactor to the bypass mode and a washing flask was inserted into the system. When the humidified acetaldehyde gas mixture was directed over the TiO_2 film, the acetaldehyde concentration rapidly increases from 1000 ppb to 6000 ppb indicating a desorption of acetaldehyde from the TiO_2 surface because water molecules are favorably adsorbed. After 2 h of dosing the concentration reaches the initial value of 1000 ppb again. Hence, crotonaldehyde is not formed under humid conditions because of the minor adsorption of acetaldehyde molecules (see Figure 5.2). Furthermore, water is a product of the aldol condensation, therefore the reaction equilibrium is shifted to the educt site. For verification of this assumption the experiment was repeated and ATR-FTIR spectra of an anatase film were recorded during acetaldehyde treatment for 2 h under dry conditions in the dark (see Figure 4.10). Bands characteristic for acetaldehyde and crotonaldehyde are observed due to the adsorption of acetaldehyde and the formation of crotonaldehyde. When changing the gas flow from dry to a humidified acetaldehyde gas mixture, the acetaldehyde and crotonaldehyde bands rapidly decrease within 5 min of dosing time evincing a fast desorption of acetaldehyde and crotonaldehyde molecules from the TiO_2 surface. Hence, acetaldehyde and crotonaldehyde are reversibly adsorbed on the TiO_2 surface, because they can be easily replaced by water molecules.

Batault *et al.*⁹ reported, that under dry conditions in the dark the adsorption of acetaldehyde molecules on the TiO_2 surface mostly occurs irreversibly, with the reversible fraction being only around 4 %. Chang *et al.*⁶³ also observed an irreversible adsorption of acetaldehyde on the SrTiO_3 surface under dry conditions. However, these authors heated their samples to 673 K and 773 K before each measurement leading to a decrease in the number of hydroxyl groups per nm^2 from 7.88 ($13.1 \mu\text{mol m}^{-2}$) at 298 K to 0.132 ($0.219 \mu\text{mol m}^{-2}$) at 873 K according to Nagao *et al.*⁶⁴ In this work, TiO_2 films were dried at RT, therefore the high number of surface hydroxyl groups prevents an irreversible adsorption of acetaldehyde on the TiO_2 surface. Batault *et al.* also observed a completely reversible physical adsorption of acetaldehyde on the TiO_2 surface using 50 % RH because of the complete surface hydroxylation, which already occurs below a

RH of 10 %.⁶⁵ According to the reaction mechanism proposed by Singh *et al.*³⁶ two acetaldehyde molecules need to be adsorbed through their oxygen lone pair on Ti^{IV} sites, in order to react with each other. Under humidified conditions the surface is completely hydroxylated and water is adsorbed, therefore acetaldehyde is not able to interact with Ti^{IV} sites and crotonaldehyde is not formed (see Figure 5.2).

El-Maazawi *et al.*³³ made similar observations, when they investigated the adsorption and the aldol condensation of acetone on the TiO_2 surface under dry and humid conditions in the dark. In the absence of water vapor 60 % of the adsorbed acetone molecules react to mesityl oxide, while under humid conditions only a minor amount of mesityl oxide is generated, because water is a product of the aldol condensation and therefore its presence does not favor the formation of mesityl oxide.

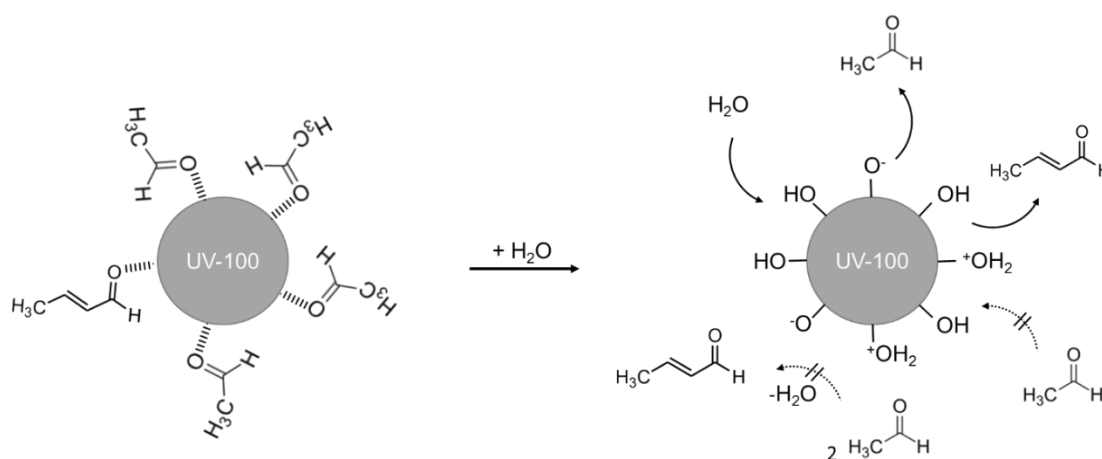


Figure 5.2: Schematic illustration of the effect of H_2O on the adsorption of acetaldehyde and the formation of crotonaldehyde on the TiO_2 surface. Reprinted from Ref.¹²

5.3 Effect of O_2 on the adsorption of acetaldehyde and the formation of crotonaldehyde

Besides the effect of water vapor, the influence of molecular O_2 on the adsorption of acetaldehyde and the formation of crotonaldehyde on the TiO_2 surface is elucidated. For this purpose, an UV-100 film was treated with acetaldehyde in the presence and absence of O_2 under dry conditions in the dark and the acetaldehyde concentration was detected at the reactor outlet. As shown in Figure 4.11, the concentration of acetaldehyde is constantly decreased from 1100 ppb to 700 ppb in O_2 and N_2 atmosphere. ATR-FTIR spectra show bands characteristic for acetaldehyde and crotonaldehyde in both, O_2 and N_2 atmosphere, which increase in intensity with acetaldehyde dosing time (see Figure 4.12). Hence, independently on the O_2 concentration acetaldehyde is adsorbed on the

5 Discussion

TiO₂ surface reacting *via* an aldol condensation to crotonaldehyde, which is desorbed from the surface and is replaced by new acetaldehyde molecules. Molecular O₂ neither has an influence on the adsorption of acetaldehyde nor on the formation of crotonaldehyde, because at the beginning of both experiments, O₂ is already adsorbed on the TiO₂ surface at oxygen vacancies (see Figure 5.3) produced by annealing at temperatures of $T > 400$ K.¹⁷ Henderson *et al.*⁶⁶ showed that O₂ becomes negatively charged upon adsorption and is stable up to 410 K, where it dissociates healing the oxygen vacancy and forming one O-adatom. Thus, O₂ is strongly adsorbed on the TiO₂ surface. Its presence during the acetaldehyde treatment does not influence the adsorption of acetaldehyde and therefore also not the formation of crotonaldehyde, since O₂ is already adsorbed on the TiO₂ surface at the beginning of both experiments.

A different trend was observed when the adsorption of isobutene on a clean rutile TiO₂ (110) surface and on a rutile TiO₂ (110) surface, that had been annealed and preadsorbed with O₂, was compared. Herein, a decreased amount of isobutene was adsorbed on the treated rutile TiO₂ (110) surface compared to the clean one because O₂ apparently blocks the adsorption sites of isobutene.⁶⁷

Idriss *et al.*⁷ observed a higher amount of acetaldehyde adsorbed on the reduced TiO₂ (001) surface compared to the oxidized TiO₂ (001) surface because in addition to Ti^{IV} sites acetaldehyde molecules might also be adsorbed on oxygen vacancies. In contrast, the formation of crotonaldehyde is facilitated on oxidized TiO₂ surfaces, because a higher number of surface oxide anions is available to initiate the aldol condensation by abstracting a proton from an adsorbed acetaldehyde molecule (see Figure 2.6).

In this study, a commercial UV-100 powder was used for the investigations, which had not been additionally treated or annealed before. Thus, the sample surfaces are similar and should not induce large differences in the adsorption of acetaldehyde and the formation of crotonaldehyde.

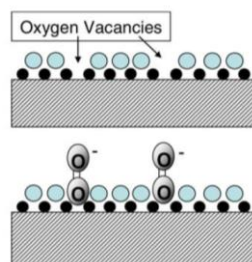


Figure 5.3: Adsorption of molecular O₂ at oxygen vacancies. Adapted from Ref.⁶⁸

5.4 Photodesorption of crotonaldehyde from the TiO₂ surface

After the adsorption and the catalytic reactions of acetaldehyde on the TiO₂ surface have been elucidated in the dark, in the following sections the photocatalytic processes occurring upon UV illumination on the TiO₂ surface are discussed. In this context, the photoinduced desorption of crotonaldehyde from the TiO₂ surface is firstly described.

The ATR-FTIR spectra shown in Figure 4.14 reveal a rapid decrease in the intensity of the bands characteristic for crotonaldehyde upon UV illumination, while the crotonaldehyde signal in the gas phase detected at the reactor outlet (see Figure 4.15) strongly increases at the beginning of the UV illumination and afterwards steadily decreases again. Thus, crotonaldehyde is desorbed from the surface into the gas phase upon UV illumination. This effect has also been observed for O₂, alkyl halides, and butene.^{68–71} Henderson *et al.*⁶⁷ showed that upon UV illumination adsorbed isobutene is desorbed from the TiO₂ surface resulting in a depletion without significant photooxidation.

One possible mechanism is the photo-thermal-desorption of crotonaldehyde from the TiO₂ surface assuming that the thermal energy released non-adiabatically by the recombination processes of photogenerated electrons and holes leads to a desorption of crotonaldehyde molecules from the TiO₂ surface (see Figure 5.4, A). This assumption has been confirmed by Berger *et al.*⁷², who reported a UV induced local heating effect in TiO₂ nanocrystals due to recombination processes. The energy released by the recombination of photogenerated charge carriers can also induce a deaggregation of TiO₂ nanoparticles according to Mendive *et al.*⁷³.

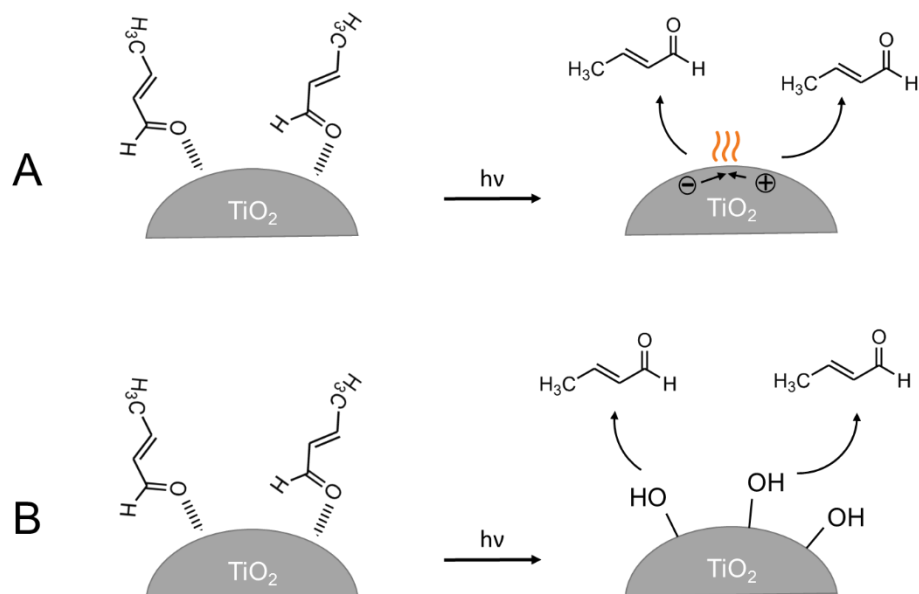


Figure 5.4: Proposed mechanisms for the desorption of crotonaldehyde from the TiO₂ surface into the gas phase upon UV illumination.

The conversion to a super hydrophilic surface structure of TiO₂ upon UV illumination could also induce a desorption of crotonaldehyde from the TiO₂ surface (see Figure 5.4, B). Upon UV illumination the TiO₂ surface becomes more hydrophilic and gradually converts into the initial less hydrophilic state when turning back to the dark mode. ¹H-NMR spectra evidenced an increase in the intensity of the signal characteristic for water molecularly adsorbed on the TiO₂ surface upon UV illumination. In the dark the signal decreased again to the initial state due to the desorption of water molecules.³¹ Sakai *et al.*⁷⁴ proposed that the photogenerated holes play a major role in the hydrophilic conversion of the TiO₂ surface. A proposed reaction mechanism for the photoinduced hydrophilicity of the TiO₂ surface is shown in Figure 5.5. Upon UV illumination the photogenerated holes are trapped as bridging oxygens atoms O_{br}^{*} leading to a weakening of the binding energy between the Ti atom and the bridging oxygen atom. Thus, water is able to break the bond resulting in the formation of two hydroxyl groups. In the dark the hydroxyl groups desorb as H₂O₂ or H₂O and O₂ from the surface.⁷⁵

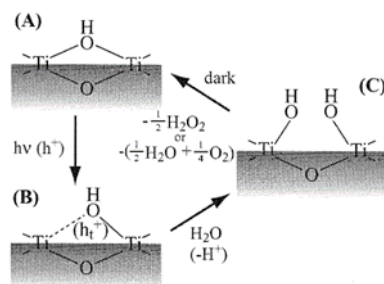


Figure 5.5: Proposed reaction mechanism for the photoinduced hydrophilicity of TiO_2 . Reprinted with permission from Ref.⁷⁵

5.5 Acetaldehyde degradation in O_2 and N_2 atmosphere

In the following section it is discussed, how molecular O_2 affects the degradation mechanism of acetaldehyde over TiO_2 . For this purpose an UV-100 film was treated with acetaldehyde in O_2 and N_2 atmosphere upon UV illumination. Figure 4.13 shows the time evolution of the acetaldehyde concentration in O_2 (left) and N_2 (right) atmosphere detected at the reactor outlet. Upon UV illumination the concentration of acetaldehyde in O_2 atmosphere decreases from 700 ppb to 580 ppb at the beginning and then remains constantly low until the end of the illumination time indicating a constant decomposition of acetaldehyde in the presence of O_2 . When the UV light is turned off the concentration increases again to its initial value evincing that acetaldehyde is not degraded anymore. In contrast, in the absence of molecular O_2 a different trend is observed. While at the beginning the concentration of acetaldehyde is as low as in O_2 atmosphere, it afterwards increases with illumination time indicating an incomplete degradation of acetaldehyde in the absence of O_2 . When the UV light is turned off, the concentration further increases to its initial value.

ATR-FTIR spectra of an UV-100 film treated with acetaldehyde in O_2 and N_2 atmosphere were recorded aiming to gain further insight into the degradation reaction of acetaldehyde on the TiO_2 surface in the presence and absence of O_2 (see Figure 4.14). These ATR-FTIR spectra reveal a decomposition of acetaldehyde upon UV illumination in O_2 atmosphere, because the intensity of the bands characteristic for acetaldehyde decrease upon UV illumination, while simultaneously new bands appear which increase in intensity with illumination time. These bands are assigned to molecular vibrations of acetate and formate. Thus, acetaldehyde is obviously degraded into acetate and formate in the presence of O_2 . These results are in accordance to the literature, where acetate and formate were also detected on the TiO_2 surface by FTIR spectroscopy during the

5 Discussion

photocatalytic acetaldehyde degradation.³⁹ Besides the formation of acetate and formate, formaldehyde and CO₂ were also detected as reaction products.^{11,39} A detailed description of the proposed degradation mechanism of acetaldehyde over TiO₂ in the presence of O₂ is shown in section 2.4.

In N₂ atmosphere acetate and formate are also generated during the first 30 min upon UV illumination, but afterwards the formation of formate decreases, while acetate is still generated. It is proposed here that at the beginning of the UV illumination O₂ is still adsorbed on the photocatalyst surface and reacts with acetaldehyde forming acetate and formate. As soon as all adsorbed O₂ molecules have been consumed, molecular O₂ is depleted and therefore acetate is not converted into formate anymore. Acetate is rather accumulated on the TiO₂ surface, therefore new acetaldehyde molecules cannot be degraded and the concentration of acetaldehyde detected at the reactor exit increases.

Szanyi *et al.*⁷⁶ investigated the photocatalytic decomposition of acetone over TiO₂ in the presence and absence of O₂ by IR spectroscopy. Upon UV illumination under anaerobic conditions acetone was incompletely decomposed and only a small amount was converted into acetate and formate. These authors proposed, that surface adsorbed O₂ had been consumed for the formation of acetate and formate and as soon as O₂ was depleted both molecules could not be decomposed into CO₂ anymore. Hence, these findings are in accordance to the results obtained in this work.

From literature it is known that O₂ is strongly adsorbed on the TiO₂ surface. Henderson *et al.*⁶⁶ have shown, that O₂ becomes negatively charged upon adsorption (see Figure 5.3). When increasing the temperature to 410 K the O₂⁻ molecule dissociates healing the V_o and forming one O-adatom. Wendt *et al.*⁷⁷ reported employing scanning tunneling microscopy (STM), that the dissociative adsorption of O₂ already occurs at RT not only on V_o, resulting in filled vacancies and isolated O-adatoms, but also on non-vacancy sites resulting in pairs of O-adatoms. It has also been shown, that the presence of surface hydroxyl groups facilitates the adsorption of O₂ molecules.⁷⁸ Hence, these results reveal that O₂ is strongly adsorbed at different TiO₂ surface sites confirming the assumption that surface adsorbed O₂ is still present on the TiO₂ surface at the beginning of the UV illumination even in N₂ atmosphere.

For a better understanding of the degradation mechanism of acetaldehyde in the absence of molecular O₂, the gas at the reactor outlet was analysed by MS during the degradation

of acetaldehyde over TiO_2 in N_2 atmosphere. Figure 4.16 and Figure 4.17 show the formation of CH_4 and CO_2 during the photocatalytic degradation of acetaldehyde. Kraeutler and Bard also observed the formation of CO_2 and CH_4 as main reaction products during the photocatalytic degradation of acetic acid over platinized TiO_2 . These authors proposed that acetic acid was converted into CO_2 and CH_4 via a photo-Kolbe reaction pathway.^{79,80} Hamid *et al.*⁸¹ also observed the formation of CH_4 and CO_2 , when aqueous acetic acid was decomposed over TiO_2 in the absence of molecular O_2 . Thus, it is proposed here that upon UV illumination and in the absence of O_2 acetaldehyde is degraded over TiO_2 forming acetate, which is decomposed into CO_2 and CH_4 . Figure 5.6 illustrates the degradation mechanism of acetaldehyde over TiO_2 in the presence and absence of O_2 . When O_2 is present at sufficiently high concentration on the TiO_2 surface acetaldehyde is constantly decomposed into acetate and formate, which is in accordance to the literature, where acetate and formate were also detected on the TiO_2 surface by FTIR spectroscopy.^{38,39} In the absence of molecular O_2 acetaldehyde is oxidized into acetate, which is accumulated on the TiO_2 surface partly reacting to CO_2 and CH_4 . Acetate is proposed to be generated by the reaction of adsorbed acetaldehyde with a bridging oxygen atom from the TiO_2 lattice. Figure 2.3 shows a schematic illustration of the TiO_2 surface consisting of bridging and terminal oxygen atoms.

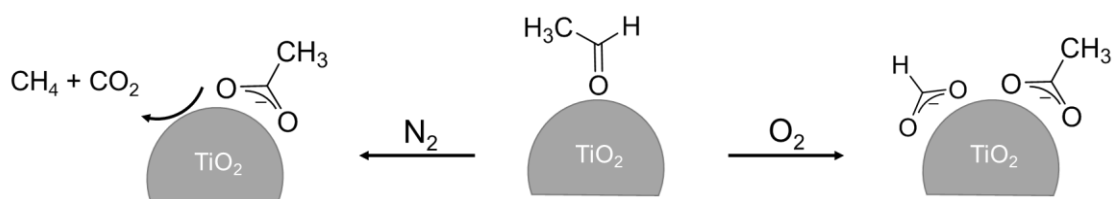
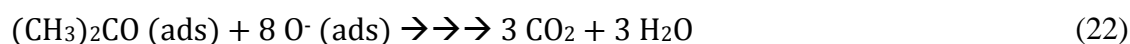


Figure 5.6: Proposed degradation mechanism of acetaldehyde over TiO_2 in the presence (left) and absence (right) of O_2 . Reprinted from Ref.¹²

Only few studies have been published suggesting that lattice oxygen atoms from the TiO_2 surface are involved in photocatalytic reactions. El-Maazawi *et al.*³³ investigated the photocatalytic degradation of acetone over dehydrated TiO_2 at different acetone coverages in the presence and absence of O_2 by FTIR spectroscopy. At low acetone coverages ($\Theta = 0.01$ monolayer) the degradation rate of acetone was much higher in the presence of O_2 as in its absence, suggesting that two mechanisms are involved in the photooxidation of acetone. In the first mechanism a photoadsorption of gas phase O_2 occurs resulting in the formation of two adsorbed O^\bullet . Upon UV illumination the

5 Discussion

photogenerated electron is trapped as Ti^{III} , which transfers one electron to an adsorbed O^{\bullet} forming O^{\bullet} that further reacts with acetone into CO_2 and H_2O (see equation 18-22):



The second mechanism involves the reaction of an adsorbed acetone with lattice oxygen atoms from the TiO_2 surface forming CO_2 and H_2O :



At low acetone coverage the reaction of acetone with adsorbed O^{\bullet} is much faster than the one with lattice oxygen atoms. In contrast, with increasing acetone coverage the reaction with lattice oxygen atoms becomes the predominant reaction pathway since the degradation rate of acetone is similar in the presence and in the absence of O_2 . Thus, lattice oxygen atoms might play a crucial role in photocatalytic processes and therefore should also be considered.

Xu *et al.*⁸² investigated the photoinduced decomposition of acetaldehyde on a reduced rutile surface in the absence of molecular O_2 at 110 K. Upon UV illumination acetaldehyde was converted into acetate and formate detected by time of flight (TOF) and temperature programmed desorption (TPD) analyses. A schematic illustration of the formation of acetate and formate on the TiO_2 surface is presented in Figure 5.7. It is proposed that adsorbed acetaldehyde reacts with bridging oxygen atoms to a bidentate structure, which either transfers one H atom to a bridging oxygen atom forming acetate or ejects CH_3^{\bullet} into the gas phase generating formate. In contrast, in the present study the formation of formate was also observed, but only at the beginning of the UV illumination when adsorbed O_2 was still present on the surface. As soon all O_2 molecules have been consumed the formation of formate decreases.

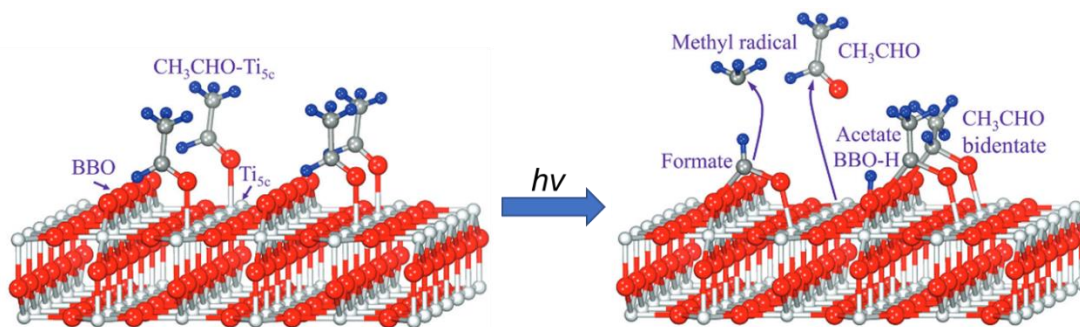
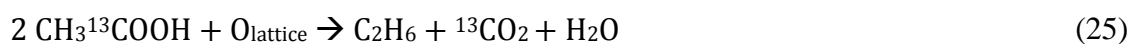


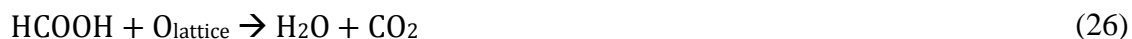
Figure 5.7: Schematic illustration of the reaction of adsorbed acetaldehyde with bridging oxygen atoms from TiO_2 forming acetate and formate upon UV illumination and in the absence of O_2 . Adapted from Ref.⁸²

Larson *et al.*⁸³ reported a photocatalytic oxidation of 2-propanol over TiO_2 forming acetone, H_2O , and CO_2 at low O_2 concentrations. These authors also proposed that lattice oxygen atoms from the TiO_2 surface were consumed for the photooxidation of 2-propanol while the gas phase O_2 was only required to replenish the remaining oxygen vacancies. Walker *et al.*⁸⁴ suggested that both, lattice oxygen atoms and gas phase O_2 are involved in the photooxidation of alkanes, while for the degradation of alcohols only lattice oxygen atoms are consumed and gas phase O_2 is only required to replenish the oxygen vacancies. Muggli *et al.*^{85,86} investigated the photocatalytic degradation of acetic acid over TiO_2 in the absence of molecular O_2 . These authors proposed that acetic acid is either decomposed into CO_2 and CH_4 , without the involvement of lattice oxygen atoms or it extracts oxygen atoms from the TiO_2 lattice to form H_2O , CO_2 , and C_2H_6 . Photocatalytic degradation experiments using $\text{CH}_3^{13}\text{COOH}$ showed the formation of $^{13}\text{CO}_2$ evincing the oxidation of the α -carbon into CO_2 while the β -carbon forms CH_4 and C_2H_6 (see equation 24 and 25). These authors proposed that the resulting oxygen vacancy is replenished by an oxygen atom supplied from the bulk.



Muggli *et al.*⁸⁷ also reported that under anaerobic conditions formic acid extracts one oxygen atom from the TiO_2 lattice to form CO_2 and H_2O (see equation 26). The resulting oxygen vacancy is replenished by an oxygen atom supplied from the bulk, which is the rate determining step in the degradation process.

5 Discussion



Hence, photocatalytic oxidation reactions proceed also in the absence of molecular O_2 and it is often suggested, that lattice oxygen atoms from the TiO_2 surface are involved in the photocatalytic degradation processes. However, isotopic studies using Ti^{18}O_2 need to be performed, in order to clearly prove this assumption. In the present work, it is proposed that upon UV illumination and in the absence of molecular O_2 acetaldehyde reacts with a bridging oxygen atom from the TiO_2 lattice forming acetate which is decomposed into CO_2 and CH_4 . According to Muggli *et al.*⁸⁵ a reaction of acetate with lattice oxygen atoms does not take place here, because lattice oxygen atoms are not required for the formation CH_4 and CO_2 .

To find out whether bridging oxygen atoms are indeed involved in the photocatalytic degradation of gaseous acetaldehyde, Ti^{16}O_2 and the isotopologues Ti^{18}O_2 were treated with acetaldehyde in the absence of molecular O_2 upon UV illumination. As illustrated in Figure 4.18, the surface structure of Ti^{18}O_2 consists of bridging oxygen atoms $^{18}\text{O}_{\text{br}}^{2-}$ and terminal oxygen atoms $^{16}\text{O}_{\text{t}}^-$ with different masses in order to distinguish between both oxygen species and to clearly evidence the incorporation of $^{18}\text{O}_{\text{br}}^{2-}$. The masses 46 m/z and 44 m/z corresponding to $\text{C}^{18}\text{O}^{16}\text{O}$ and C^{16}O_2 , respectively, were constantly detected at the reactor exit by MS. In case of bridging oxygen atoms being consumed for the formation of acetate and eventually CO_2 the $\text{C}^{18}\text{O}^{16}\text{O}/\text{C}^{16}\text{O}_2$ ratio of Ti^{18}O_2 should be increased compared to the one of Ti^{16}O_2 upon UV illumination since Ti^{18}O_2 is the only ^{18}O source. Figure 4.17 and Figure 4.19 show the C^{16}O_2 and $\text{C}^{18}\text{O}^{16}\text{O}$ evolution of Ti^{16}O_2 and Ti^{18}O_2 , respectively. When comparing the C^{16}O_2 and $\text{C}^{18}\text{O}^{16}\text{O}$ time evolution curves, both appear to be similar with the difference that the $\text{C}^{18}\text{O}^{16}\text{O}$ signal is two orders of magnitude lower than the C^{16}O_2 signal resulting from the natural abundance of the isotopologues $\text{C}^{18}\text{O}^{16}\text{O}$ in C^{16}O_2 . In the dark, both CO_2 signals of Ti^{18}O_2 and Ti^{16}O_2 are constantly low because no CO_2 is evolved. When the UV light is turned on the signals of both Ti^{18}O_2 and Ti^{16}O_2 increase strongly within the first 30 min upon illumination and afterwards steadily decrease again. This trend is in accordance to the results obtained by ATR-FTIR spectroscopy and by GC analysis. At the beginning O_2 is still adsorbed on the TiO_2 surface, reacting with acetaldehyde yielding acetate, formate, and eventually CO_2 . As soon as all the adsorbed O_2 molecules have reacted, the formation of formate and CO_2 decreases. When the UV light is turned off the CO_2 signals decrease again to the initial value. Lee *et al.*⁸⁸ and Muggli *et al.*⁸⁵⁻⁸⁷ observed a similar evolution of CO_2 , when acetic

acid and formic acid were decomposed over TiO₂ in the absence of molecular O₂. Upon UV illumination the CO₂ production quickly reached a maximum and subsequently decreased.

The C¹⁸O¹⁶O/C¹⁶O₂ ratio was calculated for Ti¹⁶O₂ and Ti¹⁸O₂ in order to prove, whether bridging oxygen atoms are involved in the formation of CO₂ during acetaldehyde degradation (see Figure 4.20). In the dark, both samples exhibit a similar ratio of 0.45 % resulting from the natural abundance of the isotopologues C¹⁸O¹⁶O in C¹⁶O₂. During the first 30 min upon UV illumination, the ratio of Ti¹⁸O₂ increases from 0.45 % to 0.56 %, remains then constant for 1 h and decreases to 0.51% until the end of illumination time. When the UV light is turned off again, the ratio decreases again to its initial value of 0.45 %. In contrast, the C¹⁸O¹⁶O/C¹⁶O₂ ratio of Ti¹⁶O₂ remains constant in the dark and upon UV illumination. The increase in the C¹⁸O¹⁶O/C¹⁶O₂ ratio of Ti¹⁸O₂ upon UV illumination clearly proves an incorporation of bridging oxygen atoms into CO₂ since Ti¹⁸O₂ is the only ¹⁸O source. Thus, the assumption of a reaction of acetaldehyde with bridging oxygen atoms forming acetate has clearly been confirmed by these isotopologues measurements. A schematic illustration of the reaction mechanism of acetaldehyde on the TiO₂ surface in the absence of O₂ is shown in Figure 5.8. Upon UV illumination the holes are trapped as O_{br}^{•-}, which subsequently react with acetaldehyde forming acetate that is further decomposed into CO₂ and CH₄. The remaining oxygen vacancy is replenished by an oxygen atom supplied from adsorbed H₂¹⁶O, because upon UV illumination the C¹⁸O¹⁶O/C¹⁶O₂ ratio of Ti¹⁸O₂ decreases. The replenished ¹⁶O_{br}²⁻ vacancy acts as new trapping site for a hole forming ¹⁶O_{br}^{•-} that again reacts with adsorbed acetaldehyde forming acetate and eventually C¹⁶O₂. Hence, a decrease in the C¹⁸O¹⁶O/C¹⁶O₂ ratio is observed, because only a limited amount of ¹⁸O_{br} is available for the reaction with acetaldehyde. Schaub *et al.*⁸⁹ confirmed the assumption of the replenishment of the oxygen vacancy by water. These authors showed that oxygen vacancies in the TiO₂ surface layer initiate the dissociation of H₂O through a transfer of one proton to a nearby oxygen atom, thus forming two hydroxyl groups per vacancy.

5 Discussion

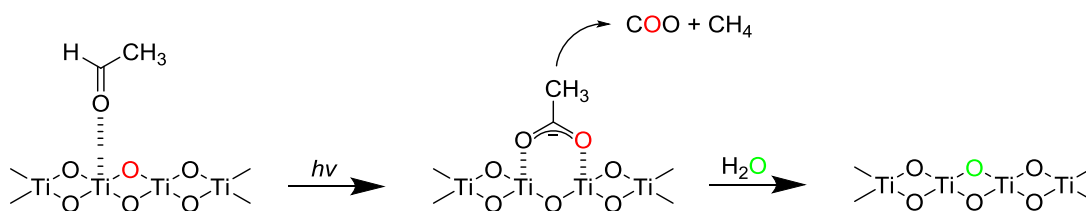


Figure 5.8: Proposed reaction mechanism of acetaldehyde with a bridging oxygen atom from the TiO_2 surface upon UV illumination and in the absence of O_2 . An adsorbed acetaldehyde molecule reacts with a bridging oxygen atom from the TiO_2 surface forming acetate and subsequently CH_4 and CO_2 . The remaining oxygen vacancy is replenished by an oxygen atom supplied from H_2O . Reprinted from Ref.⁵⁷

Montoya *et al.*^{15,27} also performed isotopic studies using Ti^{18}O_2 in liquid phase. Upon UV illumination benzene, benzaldehyde, and phenol were photocatalytically degraded over Ti^{18}O_2 and Ti^{16}O_2 under anaerobic conditions. The corresponding $\text{C}^{18}\text{O}^{16}\text{O}/\text{C}^{16}\text{O}_2$ ratios of Ti^{16}O_2 and Ti^{18}O_2 during the photocatalytic degradation of benzene are illustrated Figure 5.9.

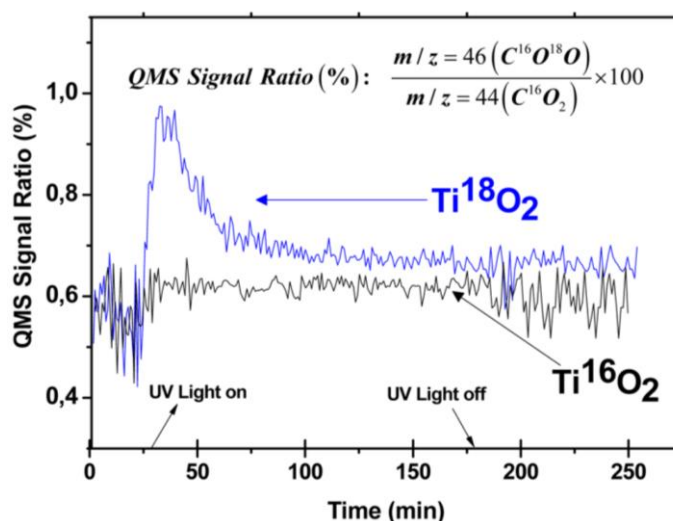


Figure 5.9: Time evolution of the $\text{C}^{18}\text{O}^{16}\text{O}/\text{C}^{16}\text{O}_2$ ratio during the photocatalytic degradation of benzene over TiO_2 . Reprinted with permission from¹⁵.

Upon UV illumination the ratio of Ti^{18}O_2 quickly increases from 0.62 % to a maximum of 0.97 %, then asymptotically decreases to 0.66 % and after 85 min remains constant until the end of illumination time. In the present work, a similar trend was observed, because at the beginning of the illumination time the $\text{C}^{18}\text{O}^{16}\text{O}/\text{C}^{16}\text{O}_2$ ratio also increased and afterwards steadily decreased until the end of illumination time. The ^{18}O enrichment in $\text{C}^{18}\text{O}^{16}\text{O}$ clearly proves an incorporation of bridging oxygen atoms into CO_2 , since Ti^{18}O_2 contains the only ^{18}O source. An ^{18}O enrichment in $\text{C}^{18}\text{O}^{16}\text{O}$ over Ti^{18}O_2 was also observed during the degradation of phenol and benzaldehyde in the absence of O_2 . It was

proposed that upon UV illumination the trapped holes $^{18}\text{O}_{\text{br}}^{\cdot-}$ in Ti^{18}O_2 react with the adsorbed probe molecules resulting in an incorporation of the $^{18}\text{O}_{\text{br}}^{\cdot-}$ into the oxidation products yielding as final product $\text{C}^{18}\text{O}^{16}\text{O}$. The remaining oxygen vacancies are healed by oxygen atoms supplied from H_2^{16}O molecules. Thus, this mechanism also assumes that the TiO_2 surface is not chemically stable, but continuously experiences chemical and electronic changes in the course of the reaction.

A further experiment that also evidences the involvement of lattice oxygen atoms in photocatalytic reactions is the degradation of cyclohexane over ^{18}O -labelled TiO_2 in the presence of $^{16}\text{O}_2$.⁹⁰ While at the beginning upon UV illumination ^{18}O -containing cyclohexanone was observed as the major reaction product, it afterwards drastically decreased because the oxygen vacancies were replenished by oxygen atoms supplied from $^{16}\text{O}_2$. The ^{16}O atoms of the newly filled vacancies reacted with cyclohexane forming ^{16}O -containing cyclohexanone. ^{18}O -containing products were also observed when toluene and *para*-xylene were photocatalytically degraded over ^{18}O -labelled TiO_2 . Hence, these studies show that the Mars-van Krevelen⁵⁰ mechanism can also be applied in photooxidation reactions at the liquid-solid interface (see section 2.5). However, when performing investigations using ^{18}O -labelled TiO_2 in the presence of $^{16}\text{O}_2$, the photoinduced oxygen exchange between lattice oxygen atoms from the TiO_2 surface and molecular O_2 should also be taken into account (see section 2.5).^{47,91,92} In the present study, the photocatalytic degradation of acetaldehyde using Ti^{18}O_2 was performed in the absence of molecular O_2 , thus a photoinduced oxygen exchange should not take place.

The number of $^{18}\text{O}_{\text{br}}^{2-}$ atoms incorporated in the evolved $\text{C}^{18}\text{O}^{16}\text{O}$ was calculated for Ti^{18}O_2 in order to figure out how many bridging oxygen atoms from the TiO_2 surface are involved in the photocatalytic degradation reaction of acetaldehyde in the absence of O_2 . For this purpose, the amount of C^{16}O_2 evolved during the degradation of acetaldehyde was calculated in the time range between 1.7 h and 5 h yielding a value of 4.29 μmol C^{16}O_2 . A further integration in the same time range was performed for the $\text{C}^{18}\text{O}^{16}\text{O}/\text{C}^{16}\text{O}_2$ ratio of Ti^{18}O_2 obtaining a value of 0.32 %. By combining these results the amount of $\text{C}^{18}\text{O}^{16}\text{O}$ evolved during acetaldehyde degradation was calculated to be 0.014 μmol $\text{C}^{18}\text{O}^{16}\text{O}$. Finally, the number of incorporated $^{18}\text{O}_{\text{br}}^{2-}$ species was calculated from the amount of $\text{C}^{18}\text{O}^{16}\text{O}$ and amounts to 8.16×10^{15} TiO_2 oxygen atoms.

5 Discussion

Montoya *et al.*¹⁵ obtained a similar value of 9.33×10^{15} bridging oxygen atoms, which were incorporated into CO_2 , during the degradation of benzene in an aqueous solution over TiO_2 under anaerobic conditions. During the POIE 4×10^{15} oxygen atoms from the TiO_2 surface were exchanged with molecular O_2 .⁹³ Hence, these results show that the number of bridging oxygen atoms exchanged during the photocatalytic reaction process is similar in liquid and in gas phase.

6 Summary and conclusions

In the present study the effect of H₂O and O₂ on the adsorption and the photocatalytic degradation of gaseous acetaldehyde over TiO₂ has been investigated for the first time in the dark and upon UV illumination at ambient temperature. In this regard, the surface processes were monitored by means of *in situ* ATR-FTIR spectroscopy, while the gas phase was analysed by GC/PID and MS. The results obtained were correlated with each other, in order to gain a deeper understanding of the adsorption and degradation mechanism of acetaldehyde on the TiO₂ surface.

ATR-FTIR spectra reveal an adsorption of acetaldehyde on the TiO₂ surface under dry conditions in the dark. Hereby, the oxygen lone pair of the carbonyl group of acetaldehyde interacts with Ti^{IV} sites, because the $\nu(\text{C}=\text{O})$ of acetaldehyde shifts from 1761 cm⁻¹ in the gas phase to lower wavenumbers of 1699 cm⁻¹.⁴¹ In addition to the adsorption of acetaldehyde, ATR-FTIR spectra show the formation of crotonaldehyde on the TiO₂ surface. When two acetaldehyde molecules are adsorbed on the TiO₂ surface, a surface catalyzed aldol condensation takes place forming crotonaldehyde and water (see Figure 6.1, left). The reaction is initiated by a bridging oxygen atom from the TiO₂ lattice abstracting one proton from an α -carbon of an adsorbed acetaldehyde molecule. The generated crotonaldehyde is also adsorbed through its oxygen lone pair on Ti^{IV} sites, because the $\nu(\text{C}=\text{O})$ of crotonaldehyde shifts from 1725 cm⁻¹ in the gas phase to 1650 cm⁻¹.⁶⁰ Thus, crotonaldehyde and acetaldehyde compete for adsorption sites, because they are both adsorbed at Ti^{IV} sites. In this study, a continuous acetaldehyde gas flow was directed over the TiO₂ surface leading to a desorption of crotonaldehyde molecules from the TiO₂ surface into the gas phase. The increased concentration of crotonaldehyde in the gas phase was detected by MS. Crotonaldehyde molecules on the TiO₂ surface were replaced by new acetaldehyde molecules, which again reacted *via* an aldol condensation to crotonaldehyde. Hence, the acetaldehyde concentration detected at the reactor outlet by GC/PID was constantly decreased.

A different trend was observed when a humidified acetaldehyde gas flow was directed over a TiO₂ film. Herein, the acetaldehyde concentration detected at the reactor outlet was shortly decreased and immediately increased to its initial value indicating that only a minor amount of acetaldehyde was adsorbed on the TiO₂ surface, because water preferably interacts with the TiO₂ surface. The strong interaction between water and TiO₂ even induced a desorption of already adsorbed acetaldehyde molecules from the TiO₂

6 Summary and conclusions

surface when water vapor was inserted into the system. The ATR-FTIR bands characteristic for acetaldehyde rapidly decreased within 5 min of dosing time evincing a fast desorption from the TiO_2 surface into the gas phase, where an increase in the concentration of acetaldehyde was observed by GC/PID. The reduced amount of acetaldehyde molecules adsorbed on the TiO_2 surface in the presence of water vapor leads to a lowering of the formation of crotonaldehyde, because acetaldehyde molecules are no longer able to react with each other (see Figure 6.1).

Hence, the adsorption of acetaldehyde and the formation of crotonaldehyde are strongly affected by the presence of water vapor. In contrast, molecular O_2 does not show an influence on the surface processes of acetaldehyde under dry conditions in the dark. In the presence and absence of O_2 the ATR-FTIR spectra and GC/PID analyses reveal an adsorption of acetaldehyde on the TiO_2 surface, followed by a reaction to crotonaldehyde, which is desorbed from the surface and is replaced by new acetaldehyde molecules that again react to crotonaldehyde. The presence of molecular O_2 during the acetaldehyde treatment does not affect the surface processes in the dark, because molecular O_2 is already strongly adsorbed on the TiO_2 surface at the beginning of both experiments and does neither influence the aldol condensation nor the adsorption and desorption of acetaldehyde and crotonaldehyde, respectively.

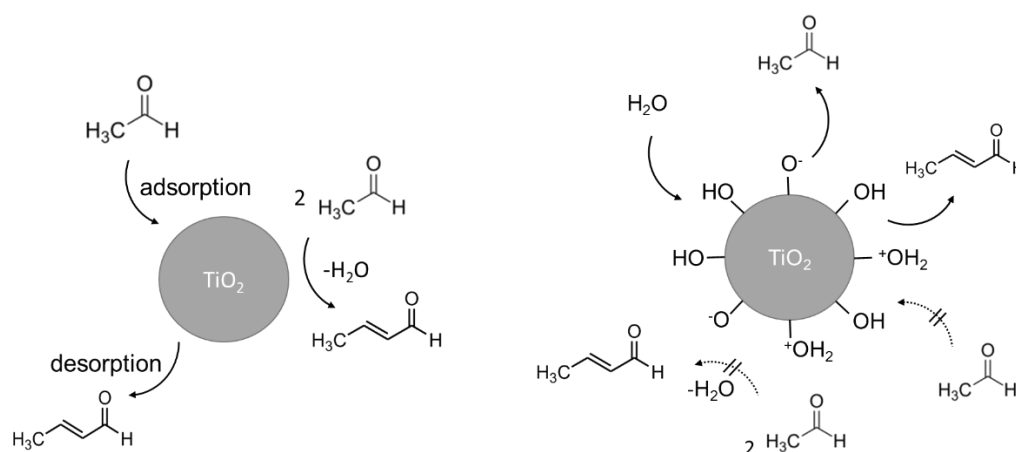


Figure 6.1: Adsorption and surface catalyzed reactions of acetaldehyde on the TiO_2 surface under dry (left) and humidified conditions (right) in the dark. Reprinted from Ref.¹²

Upon UV illumination the ATR-FTIR spectra recorded in O_2 and N_2 atmosphere reveal a decrease in intensity of the bands characteristic for crotonaldehyde, while simultaneously the concentration of crotonaldehyde in the gas phase detected at the reactor outlet by MS increases. Hence, crotonaldehyde is desorbed from the TiO_2 surface

into the gas phase upon UV illumination. One possible mechanism is the photo-thermal-desorption of crotonaldehyde from the TiO₂ surface assuming that the thermal energy released non-adiabatically by the recombination processes of photogenerated electrons and holes leads to a desorption of crotonaldehyde molecules from the TiO₂ surface. Another possibility is, that the conversion to a super hydrophilic surface structure of TiO₂ upon UV illumination induces a desorption of crotonaldehyde from the TiO₂ surface.

In addition to crotonaldehyde, acetaldehyde is also present on the TiO₂ surface. Upon UV illumination molecular O₂ affects the degradation mechanism of acetaldehyde on the TiO₂ surface (see Figure 6.2). GC/PID results indicate a constant degradation of acetaldehyde in the presence of O₂, while in the absence of O₂ an incomplete degradation of acetaldehyde occurs. ATR-FTIR spectra reveal a degradation of acetaldehyde on the TiO₂ surface forming acetate and formate in the presence of O₂. In N₂ atmosphere adsorbed O₂ is still present on the TiO₂ surface at the beginning of the UV illumination reacting with acetaldehyde into acetate, formate, and CO₂. As soon as all adsorbed O₂ molecules have been consumed the formation of formate and CO₂ decreases, while acetate is still observed on the TiO₂ surface. It is proposed here, that acetate is accumulated on the TiO₂ surface and partly decomposes into CO₂ and CH₄, which were detected in the gas phase by MS.

In the absence of O₂ it is proposed that an adsorbed acetaldehyde molecule reacts with a bridging oxygen atom from the TiO₂ lattice forming acetate which is subsequently decomposed into CH₄ and CO₂ (see Figure 6.2). Thus, the evolved CO₂ should contain a bridging oxygen atom from the TiO₂ lattice in case bridging oxygen atoms are involved in the photocatalytic degradation process of acetaldehyde. For proving this assumption acetaldehyde was degraded over Ti¹⁶O₂ (UV-100) and Ti¹⁸O₂ in the absence of O₂ and the evolved C¹⁶O₂ (44 m/z) and C¹⁸O¹⁶O (46 m/z) were constantly detected at the reactor outlet by MS. The C¹⁸O¹⁶O/C¹⁶O₂ ratio of Ti¹⁶O₂ and Ti¹⁸O₂ was calculated in order to determine whether bridging oxygen atoms are incorporated into CO₂. Upon UV illumination the C¹⁸O¹⁶O/C¹⁶O₂ ratio of Ti¹⁸O₂ increased, which clearly proves an incorporation of bridging oxygen atoms into CO₂, since Ti¹⁸O₂ contains the only ¹⁸O source. In contrast, the C¹⁸O¹⁶O/C¹⁶O₂ ratio of Ti¹⁶O₂ remains constant in the dark and upon UV illumination. It is therefore proposed here, that upon UV illumination holes are trapped as ¹⁸O_{br}[•], which react with adsorbed acetaldehyde forming acetate that is further decomposed into C¹⁸O¹⁶O and CH₄. The remaining oxygen vacancy is replenished by an

6 Summary and conclusions

oxygen atom supplied from adsorbed H_2^{16}O , because upon UV illumination the $\text{C}^{18}\text{O}^{16}\text{O}/\text{C}^{16}\text{O}_2$ ratio of Ti^{18}O_2 decreases. The replenished $^{16}\text{O}_{\text{br}}^{2-}$ vacancy acts as new trapping site for a hole forming $^{16}\text{O}_{\text{br}}^{\cdot-}$ that again reacts with adsorbed acetaldehyde forming acetate and eventually C^{16}O_2 . Thus, a decrease in the $\text{C}^{18}\text{O}^{16}\text{O}/\text{C}^{16}\text{O}_2$ ratio is observed, because only a limited amount of $^{18}\text{O}_{\text{br}}^{2-}$ is available for the reaction with acetaldehyde. Hence, in this work it was shown for the first time that bridging oxygen atoms from the TiO_2 lattice are involved in the photocatalytic degradation process of gaseous acetaldehyde. Therefore, besides O_2 and H_2O the involvement of lattice oxygen atoms from the TiO_2 surface also need to be considered in photocatalytic reactions.

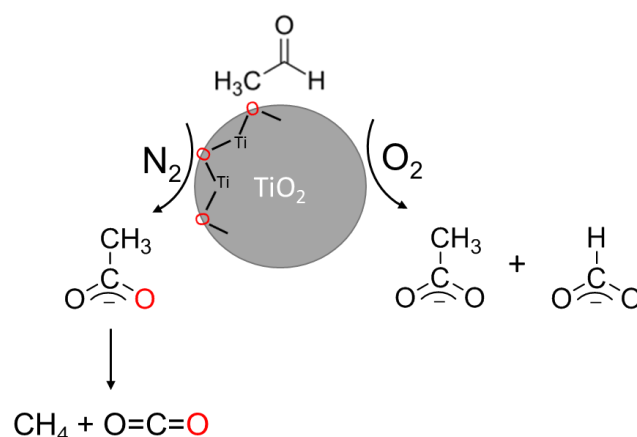


Figure 6.2: Proposed reaction mechanism for the photocatalytic degradation of acetaldehyde over TiO_2 in the presence and absence of O_2 . Reprinted from Ref.¹²

7 References

- (1) Meroni, D.; Ardizzone, S.; Cappelletti, G.; Oliva, C.; Ceotto, M.; Poelman, D.; Poelman, H. *Catal. Today* **2011**, *161* (1), 169–174.
- (2) European Agency for Safety and Health at Work., European Risk Observatory Report. Exploratory Survey of Occupational Exposure Limits for Carcinogens, Mutagens and Reprotoxic substances at EU Member States Level, **2009**; <https://osha.europa.eu/en/publications/reports/548OELs/view>.
- (3) *Occupational Safety and Health Administration (OSHA), Permissible Exposure Limits, Occupational Safety and Health Administration*; Washington, DC, **2005**.
- (4) Sopyan, I.; Watanabe, M.; Murasawa, S.; Hashimoto, K.; Fujishima, A. *J. Photochem. Photobiol. A Chem.* **1996**, *98* (1), 79–86.
- (5) Atitar, M. F.; Belhadj, H.; Dillert, R.; Bahnemann, D. W. *The Relevance of ATR-FTIR Spectroscopy in Semiconductor Photocatalysis*; Larramendy, M. L., Soloneski, S. B. T.-E. P. in the E.-C. and F. I., Eds.; InTech: Rijeka, **2015**.
- (6) Mendive, C. B.; Bredow, T.; Blesa, M. A.; Bahnemann, D. W. *Phys. Chem. Chem. Phys.* **2006**, *8* (27), 3232–3247.
- (7) Idriss, H.; Barteau, M. A. *Catal. Letters* **1996**, *40* (3), 147–153.
- (8) Idriss, H.; Diagne, C.; Hindermann, J. P.; Kiennemann, A.; Barteau, M. A. *J. Catal.* **1995**, *155* (2), 219–237.
- (9) Batault, F.; Thevenet, F.; Hequet, V.; Rillard, C.; Le Coq, L.; Locoge, N. *Chem. Eng. J.* **2015**, *264*, 197–210.
- (10) Muggli, D. S.; McCue, J. T.; Falconer, J. L. *J. Catal.* **1998**, *173* (2), 470–483.
- (11) Ohko, Y.; Tryk, D. A.; Hashimoto, K.; Fujishima, A. *J. Phys. Chem. B* **1998**, *102* (15), 2699–2704.
- (12) Melchers, S.; Schneider, J.; Bahnemann, D. W. *Catalysts* **2018**, *8* (417).
- (13) Sonntag, C. von. *Free-Radical-Induced DNA Damage and Its Repair*; Schreck, S., Ed.; Springer-Verlag: Berlin/Heidelberg, **2006**.
- (14) Henderson, M. A. *Surf. Sci. Rep.* **2011**, *66* (6), 185–297.
- (15) Montoya, J. F.; Ivanova, I.; Dillert, R.; Bahnemann, D. W.; Salvador, P.; Peral, J. *J. Phys. Chem. Lett.* **2013**, *4* (9), 1415–1422.
- (16) Idriss, H.; Légare, P.; Maire, G. *Surf. Sci.* **2002**, *515* (2), 413–420.
- (17) Linsebigler, A.; Lu, G.; Yates, J. T. *J. Phys. Chem.* **1996**, *100* (16), 6631–6636.
- (18) Dambournet, D.; Belharouak, I.; Amine, K. *Chem. Mater.* **2010**, *22* (3), 1173–1179.
- (19) Tang, H.; Berger, H.; Schmid, P. E.; Lévy, F.; Burri, G. *Solid State Commun.* **1993**, *87* (9), 847–850.
- (20) Pascual, J.; Camassel, J.; Mathieu, H. *Fine-Structure In the Intrinsic Absorption-Edge Of TiO2*; **1978**; Vol. 18.

7 References

- (21) Di Paola, A.; Bellardita, M.; Palmisano, L. *Brookite, the Least Known TiO₂ Photocatalyst*; **2013**; Vol. 3.
- (22) Schneider, J.; Matsuoka, M.; Takeuchi, M.; Zhang, J.; Horiuchi, Y.; Anpo, M.; Bahnemann, D. W. *Chem. Rev.* **2014**, *114* (19), 9919–9986.
- (23) Serpone, N.; Lawless, D.; Khairutdinov, R.; Pelizzetti, E. *J. Phys. Chem.* **1995**, *99* (45), 16655–16661.
- (24) Hennig, H. *Angew. Chemie Int. Ed.* **2015**, *54* (15), 4429.
- (25) Wood, P. M. *Biochem. J.* **1988**, *253* (1), 287 LP-289.
- (26) Diebold, U. *Surf. Sci. Rep.* **2003**, *48* (5), 53–229.
- (27) Montoya, J. F.; Bahnemann, D. W.; José, P.; Pedro, S. *ChemPhysChem* **2014**, *15* (11), 2311–2320.
- (28) Nosaka, A. Y.; Nishino, J.; Fujiwara, T.; Ikegami, T.; Yagi, H.; Akutsu, H.; Nosaka, Y. *J. Phys. Chem. B* **2006**, *110* (16), 8380–8385.
- (29) Nováková, J. *Catal. Rev.* **1971**, *4* (1), 77–113.
- (30) Sato, S. *J. Phys. Chem.* **1987**, *91* (11), 2895–2897.
- (31) Nosaka, A. Y.; Kojima, E.; Fujiwara, T.; Yagi, H.; Akutsu, H.; Nosaka, Y. *J. Phys. Chem. B* **2003**, *107* (44), 12042–12044.
- (32) János, R.; Kiss, J. *Adsorption and surface reactions of acetaldehyde on TiO₂, CeO₂ and Al₂O₃*; 2005; Vol. 287.
- (33) El-Maazawi, M.; Finken, A. N.; Nair, A. B.; Grassian, V. H. *J. Catal.* **2000**, *191* (1), 138–146.
- (34) Ordonsky, V. V.; Sushkevich, V. L.; Ivanova, I. I. *J. Mol. Catal. A Chem.* **2010**, *333* (1), 85–93.
- (35) Raskó, J.; Kiss, J. *Catal. Letters* **2005**, *101* (1), 71–77.
- (36) Singh, M.; Zhou, N.; Paul, D. K.; Klabunde, K. J. *J. Catal.* **2008**, *260* (2), 371–379.
- (37) Raskó, J.; Kecskés, T.; Kiss, J. *Appl. Catal. A Gen.* **2005**, *287* (2), 244–251.
- (38) Topalian, Z.; Stefanov, B. I.; Granqvist, C. G.; Österlund, L. *J. Catal.* **2013**, *307*, 265–274.
- (39) Hauchecorne, B.; Terrens, D.; Verbruggen, S.; Martens, J. A.; Van Langenhove, H.; Demeestere, K.; Lenaerts, S. *Appl. Catal. B Environ.* **2011**, *106* (3–4), 630–638.
- (40) Sauer, M. L.; Ollis, D. F. *J. Catal.* **1996**, *158* (2), 570–582.
- (41) Nimlos, M. R.; Wolfrum, E. J.; Brewer, M. L.; Fennell, J. A.; Bintner, G. *Environ. Sci. Technol.* **1996**, *30* (10), 3102–3110.
- (42) Muggli, D. S.; Lowery, K. H.; Falconer, J. L. *J. Catal.* **1998**, *180* (2), 111–122.
- (43) Guzman, F.; Chuang, S. S. C. *J. Am. Chem. Soc.* **2010**, *132* (5), 1502–1503.

- (44) Ao, C. H.; Lee, S. C.; Yu, J. Z.; Xu, J. H. *Appl. Catal. B Environ.* **2004**, *54* (1), 41–50.
- (45) Peral, J.; Ollis, D. F. *J. Catal.* **1992**, *136* (2), 554–565.
- (46) Yang, J.; Li, D.; Zhang, Z.; Li, Q.; Wang, H. *J. Photochem. Photobiol. A Chem.* **2000**, *137* (2), 197–202.
- (47) Pichat, P.; Courbon, H.; Enriquez, R.; Tan, T. T. Y.; Amal, R. *Res. Chem. Intermed.* **2007**, *33* (3), 239–250.
- (48) Montoya, J. F.; Peral, J.; Salvador, P. *ChemPhysChem* **2011**, *12* (5), 901–907.
- (49) Almeida, A. R.; Moulijn, J. A.; Mul, G. *J. Phys. Chem. C* **2011**, *115* (4), 1330–1338.
- (50) Mars, P.; van Krevelen, D. W. *Chem. Eng. Sci.* **1954**, *3*, 41–59.
- (51) Brunauer, S.; Emmett, P. H.; Teller, E. *J. Am. Chem. Soc.* **1938**, *60* (2), 309–319.
- (52) Harrick, N. J. *J. Phys. Chem.* **1960**, *64* (9), 1110–1114.
- (53) Fahrenfort, J. *Spectrochim. Acta* **1961**, *17* (7), 698–709.
- (54) Hug, S. J.; Sulzberger, B. *Langmuir* **1994**, *10* (12), 3587–3597.
- (55) Frank, O.; Zukalova, M.; Laskova, B.; Kurti, J.; Koltai, J.; Kavan, L. *Phys. Chem. Chem. Phys.* **2012**, *14* (42), 14567–14572.
- (56) Kavan, L.; Zukalova, M.; Ferus, M.; Kurti, J.; Koltai, J.; Civis, S. *Phys. Chem. Chem. Phys.* **2011**, *13* (24), 11583–11586.
- (57) Melchers, S.; Schneider, J.; W. Bahnemann, D. *Catal Today*, **2018**. (in press)
- (58) Stefanov, B. I.; Topalian, Z.; Granqvist, C. G.; Österlund, L. *J. Mol. Catal. A Chem.* **2014**, *381*, 77–88.
- (59) Rekoske, J. E.; Barteau, M. A. *Langmuir* **1999**, *15* (6), 2061–2070.
- (60) Lochar, V.; Smoláková, L. *React. Kinet. Catal. Lett.* **2009**, *96* (1), 117–123.
- (61) Sofianou, M.-V.; Psycharis, V.; Boukos, N.; Vaimakis, T.; Yu, J.; Dillert, R.; Bahnemann, D.; Trapalis, C. *Appl. Catal. B Environ.* **2013**, *142–143*, 761–768.
- (62) Horikoshi, S.; Kajitani, M.; Horikoshi, N.; Dillert, R.; Bahnemann, D. W. *J. Photochem. Photobiol. A Chem.* **2008**, *193* (2), 284–287.
- (63) Chang, C.-A.; Ray, B.; Paul, D. K.; Demydov, D.; Klabunde, K. J. *J. Mol. Catal. A Chem.* **2008**, *281* (1), 99–106.
- (64) Nagao, M.; Suda, Y. *Langmuir* **1989**, *5* (1), 42–47.
- (65) Coronado, J. M.; Zorn, M. E.; Tejedor-Tejedor, I.; Anderson, M. A. *Appl. Catal. B Environ.* **2003**, *43* (4), 329–344.
- (66) Henderson, M. A.; Epling, W. S.; Perkins, C. L.; Peden, C. H. F.; Diebold, U. *J. Phys. Chem. B* **1999**, *103* (25), 5328–5337.
- (67) Henderson, M. A. *J. Phys. Chem. C* **2013**, *117* (27), 14113–14124.

7 References

- (68) Yates, J. T. *Surf. Sci.* **2009**, *603* (10), 1605–1612.
- (69) Henderson, M. A. *J. Phys. Chem. C* **2013**, *117* (45), 23840–23847.
- (70) Kim, S. H.; Stair, P. C.; Weitz, E. *Chem. Phys. Lett.* **1999**, *302* (5), 511–516.
- (71) Kim, S. H.; Stair, P. C.; Weitz, E. *J. Chem. Phys.* **1998**, *108* (12), 5080–5088.
- (72) Berger, T.; Diwald, O.; Knözinger, E.; Sterrer, M.; Yates Jr, J. T. *Phys. Chem. Chem. Phys.* **2006**, *8* (15), 1822–1826.
- (73) Mendive, C. B.; Hansmann, D.; Bredow, T.; Bahnemann, D. *J. Phys. Chem. C* **2011**, *115* (40), 19676–19685.
- (74) Sakai, N.; Fujishima, A.; Watanabe, T.; Hashimoto, K. *J. Phys. Chem. B* **2001**, *105* (15), 3023–3026.
- (75) Sakai, N.; Fujishima, A.; Watanabe, T.; Hashimoto, K. *J. Phys. Chem. B* **2003**, *107* (4), 1028–1035.
- (76) Szanyi, J.; Kwak, J. H. *J. Mol. Catal. A Chem.* **2015**, *406*, 213–223.
- (77) Wendt, S.; Sprunger, P. T.; Lira, E.; Madsen, G. K. H.; Li, Z.; Hansen, J. Ø.; Matthiesen, J.; Blekinge-Rasmussen, A.; Lægsgaard, E.; Hammer, B.; Besenbacher, F. *Science (80-.)* **2008**, *320* (5884), 1755 LP-1759.
- (78) Liu, L. M.; McAllister, B.; Ye, H. Q.; Hu, P. *J. Am. Chem. Soc.* **2006**, *128* (12), 4017–4022.
- (79) Kraeutler, B.; Bard, A. J. *J. Am. Chem. Soc.* **1978**, *100* (7), 2239–2240.
- (80) Kraeutler, B.; Bard, A. J. *J. Am. Chem. Soc.* **1978**, *100* (19), 5985–5992.
- (81) Hamid, S.; Ivanova, I.; Jeon, T. H.; Dillert, R.; Choi, W.; Bahnemann, D. W. *J. Catal.* **2017**, *349*, 128–135.
- (82) Xu, C.; Yang, W.; Guo, Q.; Dai, D.; Yang, X. *Phys. Chem. Chem. Phys.* **2016**, *18* (45), 30982–30989.
- (83) Larson, S. A.; Widegren, J. A.; Falconer, J. L. *J. Catal.* **1995**, *157* (2), 611–625.
- (84) Walker, A.; Formenti, M.; Meriaudeau, P.; Teichner, S. J. *J. Catal.* **1977**, *50* (2), 237–243.
- (85) Muggli, D. S.; Falconer, J. L. *J. Catal.* **1999**, *187* (1), 230–237.
- (86) Muggli, D. S.; Keyser, S. A.; Falconer, J. L. *Catal. Letters* **1998**, *55* (3), 129–135.
- (87) Muggli, D. S.; Falconer, J. L. *J. Catal.* **2000**, *191* (2), 318–325.
- (88) Lee, G. D.; Falconer, J. L. *Catal. Letters* **2000**, *70* (3), 145–148.
- (89) Schaub, R.; Thostrup, P.; Lopez, N.; Lægsgaard, E.; Stensgaard, I.; Nørskov, J. K.; Besenbacher, F. *Phys. Rev. Lett.* **2001**, *87* (26), 266104.
- (90) Choi, J.; Kang, D.; Lee, K. H.; Lee, B.; Kim, K. J.; Hur, N. H. *RSC Adv.* **2013**, *3* (24), 9402–9407.
- (91) Formenti, M.; Courbon, H.; Juillet, F.; Lissatchenko, A.; Martin, J. R.; Meriaudeau, P.; Teichner, S. J. *J. Vac. Sci. Technol.* **1972**, *9* (2), 947–952.

- (92) Courbon, H.; Formenti, M.; Pichat, P. *J. Phys. Chem.* **1977**, *81* (6), 550–554.
- (93) Mikhaylov, R. V; Lisachenko, A. A.; Titov, V. V. *J. Phys. Chem. C* **2012**, *116* (44), 23332–23341.

8 Publications

S. Melchers, J. Schneider, D. W. Bahnemann, Isotopic Studies on the Degradation of Acetaldehyde on Anatase Surfaces. *Catalysis Today* **2018**. (in press)

S. Melchers, J. Schneider, A. V. Emeline, D. W. Bahnemann, Effect of O₂ on the Adsorption and Degradation of Acetaldehyde on Anatase Surfaces – An in situ ATR-FTIR Study. *Catalysts* **2018**, 8, 417.

S. Melchers, Y. AlSalka, J. Schneider, D. W. Bahnemann, Studies on the Adsorption and Photocatalytic Degradation of an Eu^{III}(TTFA)₃(MePhTerpy) Complex on the TiO₂ Surface. *J Photochem Photobiol A : Chem* **2018**, 364, 303.

C. Haisch, C. Günnemann, S. Melchers, M. Fleisch, J. Schneider, A. V. Emeline, D. W. Bahnemann, Irreversible surface changes upon n-type doping – A photoelectrochemical study on rutile single crystals. *Electrochimica Acta* **2018**, 280, 278.

H. Belhadj, S. Melchers, P. K. J. Robertson, D. W. Bahnemann, Pathways of the photocatalytic reaction of acetate in H₂O and D₂O: A combined EPR and ATR-FTIR study. *J Catal* **2016**, 344, 831.

S. Melchers, T. Uesbeck, O. Winter, D. Eder, Effect of Aluminium Ion Incorporation on the Bioactivity and Structure in Mesoporous Bioactive Glasses. *Chem Mater* **2016**, 28, 3254.

9 Curriculum vitae

Personal data

Name	Melchers, Stephanie
Date of birth	10.10.1988
Place of birth	Bremen, Germany

Education

Since 09/2015	PhD student at the Institute of Technical Chemistry at the Leibniz University of Hanover: “Adsorption and Transformation of Acetaldehyde on the TiO ₂ surface”.
03/2014 – 09/2014	Master Thesis at the Institute of Physical Chemistry at the University of Münster: “Synthesis and Characterization of Metal Ion Doped Bioactive Glasses”.
10/2012 – 09/2014	Master of Science (M. Sc.) in Chemistry at the University of Münster.
10/2009 – 09/2012	Bachelor of Science (B. Sc.) in Chemistry at the University of Münster.
06/2008	Abitur at Altes Gymnasium Bremen.